



Host Galaxy Properties and Offset Distributions of Fast Radio Bursts: Implications for Their Progenitors

Kasper E. Heintz¹, J. Xavier Prochaska^{2,3}, Sunil Simha², Emma Platts⁴, Wen-fai Fong⁵, Nicolas Tejos⁶,
 Stuart D. Ryder^{7,8}, Kshitij Aggerwal^{9,10}, Shivani Bhandari¹¹, Cherie K. Day^{11,12}, Adam T. Deller¹²,
 Charles D. Kilpatrick¹³, Casey J. Law¹⁴, Jean-Pierre Macquart^{15,17}, Alexandra Mannings², Lachlan J. Marnoch^{7,8,11},
 Elaine M. Sadler^{11,16}, and Ryan M. Shannon¹²

¹ Centre for Astrophysics and Cosmology, Science Institute, University of Iceland, Dunhagi 5, 107 Reykjavík, Iceland; keh14@hi.is

² University of California—Santa Cruz, 1156 High Street, Santa Cruz, CA 95064, USA

³ Kavli Institute for the Physics and Mathematics of the Universe (Kavli IPMU), 5-1-5 Kashiwanoha, Kashiwa, 277-8583, Japan

⁴ High Energy Physics, Cosmology & Astrophysics Theory (HEPCAT) group, Department of Mathematics and Applied Mathematics, University of Cape Town, South Africa

⁵ Center for Interdisciplinary Exploration and Research in Astrophysics and Department of Physics and Astronomy, Northwestern University, 2145 Sheridan Road, Evanston, IL 60208-3112, USA

⁶ Instituto de Física, Pontificia Universidad Católica de Valparaíso, Casilla 4059, Valparaíso, Chile

⁷ Department of Physics & Astronomy, Macquarie University, NSW 2109, Australia

⁸ Astronomy, Astrophysics and Astrophotonics Research Centre, Macquarie University, Sydney, NSW 2109, Australia

⁹ Department of Physics and Astronomy, West Virginia University, Morgantown, WV 26506, USA

¹⁰ Center for Gravitational Waves and Cosmology, West Virginia University, Chestnut Ridge Research Building, Morgantown, WV, USA

¹¹ Australia Telescope National Facility, CSIRO Astronomy and Space Science, P.O. Box 76, Epping, NSW 1710, Australia

¹² Centre for Astrophysics and Supercomputing, Swinburne University of Technology, Hawthorn, VIC 3122, Australia

¹³ Department of Astronomy and Astrophysics, University of California, Santa Cruz, CA 95064, USA

¹⁴ Cahill Center for Astronomy and Astrophysics, MC 249-17 California Institute of Technology, Pasadena, CA 91125, USA

¹⁵ International Centre for Radio Astronomy Research, Curtin University, Bentley WA 6102, Australia

¹⁶ Sydney Institute for Astronomy, School of Physics A28, The University of Sydney, NSW 2006, Australia

Received 2020 July 1; revised 2020 September 6; accepted 2020 September 8; published 2020 November 12

Abstract

We present observations and detailed characterizations of five new host galaxies of fast radio bursts (FRBs) discovered with the Australian Square Kilometre Array Pathfinder (ASKAP) and localized to $\lesssim 1''$. Combining these galaxies with FRB hosts from the literature, we introduce criteria based on the probability of chance coincidence to define a subsample of 10 highly confident associations (at $z = 0.03\text{--}0.52$), 3 of which correspond to known repeating FRBs. Overall, the FRB-host galaxies exhibit a broad, continuous range of color ($M_u - M_r = 0.9\text{--}2.0$), stellar mass ($M_* = 10^8 - 6 \times 10^{10} M_\odot$), and star formation rate (SFR = $0.05\text{--}10 M_\odot \text{ yr}^{-1}$) spanning the full parameter space occupied by $z < 0.5$ galaxies. However, they do not track the color–magnitude, SFR– M_* , nor BPT diagrams of field galaxies surveyed at similar redshifts. There is an excess of “green valley” galaxies and an excess of emission-line ratios indicative of a harder radiation field than that generated by star formation alone. From the observed stellar mass distribution, we rule out the hypothesis that FRBs strictly track stellar mass in galaxies ($>99\%$ c.l.). We measure a median offset of 3.3 kpc from the FRB to the estimated center of the host galaxies and compare the host-burst offset distribution and other properties with the distributions of long- and short-duration gamma-ray bursts (LGRBs and SGRBs), core-collapse supernovae (CC-SNe), and SNe Ia. This analysis rules out galaxies hosting LGRBs (faint, star-forming galaxies) as common hosts for FRBs ($>95\%$ c.l.). Other transient channels (SGRBs, CC-, and SNe Ia) have host-galaxy properties and offsets consistent with the FRB distributions. All of the data and derived quantities are made publicly available on a dedicated website and repository.

Unified Astronomy Thesaurus concepts: Galaxies (573); Interstellar medium (847); Star formation (1569); Extragalactic radio sources (508); Radio bursts (1339); Magnetars (992)

1. Introduction

The transients classified as fast radio bursts (FRBs) and their progenitors constitute one of the major puzzles in contemporary astrophysics (see Cordes & Chatterjee 2019; Petroff et al. 2019, for recent reviews). FRBs are brief (~ 1 ms), but bright (> 1 Jy ms) radio-pulse events, similar in nature to pulsars, although their extragalactic origin (Thornton et al. 2013) implies much higher energies. Despite being first detected more than a decade ago (Lorimer et al. 2007), the physical engines powering FRBs still remain a mystery, but a plethora of origins has been proposed (see e.g., Platts et al. 2019, for a compendium).

Nevertheless, FRBs have already been demonstrated to be powerful cosmological probes. Similar to how UV or optically bright cosmic beacons such as quasars and gamma-ray burst (GRB) afterglows have been paramount in the study of the interstellar and intergalactic gas properties at high redshifts (Wolfe et al. 2005; Fynbo et al. 2009), FRBs have revolutionized the studies of the “cosmic web” between galaxies (Macquart et al. 2020; Simha et al. 2020), the diffuse ionized gas in extragalactic halos (McQuinn 2014; Prochaska & Zheng 2019; Prochaska et al. 2019a), and the interstellar and circumgalactic media of their hosts (Tendulkar et al. 2017; Chittidi et al. 2020). Most notably, FRBs can be used to provide a census of the baryonic content that is in a highly diffuse state and therefore difficult to detect with any other approach (Macquart et al. 2020).

¹⁷ Deceased.

Until recently, the main issue hindering any significant progress has been the generally poor localizations of the events. The first decade of FRB searches was undertaken with telescopes that had localization regions $\gg 1$ arcmin². This is inhibited by the seeming lack of “afterglows” analogous to those observed for GRBs (Petroff et al. 2017; Bhandari et al. 2018; Chen et al. 2020) and associated supernova-like transient counterparts (Marnoch et al. 2020). A precise localization ($\sim 1''$) of the burst itself is thus required to robustly identify the associated host galaxy (Eftekhari & Berger 2017).

The first unique identification of an FRB-host galaxy was based on direct interferometric localization of the repeat bursts from FRB 121102 (Spitler et al. 2016). Follow-up observations revealed a faint, actively star-forming (SF), low-mass galaxy at $z = 0.1927$ (Chatterjee et al. 2017; Tendulkar et al. 2017). The resemblance to the hosts of long-duration GRBs and super-luminous supernovae (SLSNe) promoted “young” flaring magnetar models as the origin of the repeat bursts (e.g., Metzger et al. 2017; Margalit & Metzger 2018). However, it is now clear that the host galaxy of FRB 121102 is anomalous compared to other FRB hosts (e.g., Bannister et al. 2019; Li et al. 2019; Bhandari et al. 2020b). Recently, another repeating FRB, FRB 180916, was localized to an SF region in a nearby spiral galaxy (Marcote et al. 2020), showing properties in stark contrast to the host of FRB 121102.

The Commensal Real-Time ASKAP Fast Transients (CRAFT; Macquart et al. 2010) survey has operated the Australian Square Kilometre Array Pathfinder (ASKAP) in incoherent-sum (ICS) mode since 2018, and now routinely provides \sim arcsecond localizations of single-pulse FRBs. This led to the discovery of the first two host galaxies associated with apparently one-off FRBs (Bannister et al. 2019; Prochaska et al. 2019a), and based on the first preliminary study of ASKAP-detected FRBs (Bhandari et al. 2020b, see also Li & Zhang 2020), it is now clear that the majority of FRB hosts are instead massive galaxies with older stellar populations. This suggests that FRBs reside in diverse environments, even for the proposed subpopulation of repeating bursts. The progenitors of FRBs (and astronomical transients in general) are likely linked to specific stellar populations and galactic environments, so detailed characterizations of their host galaxies allow us to constrain the nature of these events and their likely progenitor channels (akin to how the host properties of GRBs aided in constraining their progenitors, e.g., Fruchter et al. 2006; Yoon et al. 2006).

In this paper, we present the first comprehensive and statistical analyses of the population of galaxies hosting FRBs. These include detailed characterizations of five new host galaxies of accurately localized FRBs detected by ASKAP. Combined with all previously identified FRB hosts reported in the literature, our sample comprises a total of 13 host galaxies. We measure the physical properties of the majority of the FRB hosts in our sample based on existing and newly obtained spectroscopic and photometric data.

Throughout the paper, we distinguish between host galaxies of repeating FRBs and apparently nonrepeating, one-off bursts to investigate any distinct characteristics between the host populations of the two apparent types of FRBs. We first compare the observed FRB-host properties to those of field galaxies to examine how the FRB hosts are drawn from the underlying galaxy population. We then investigate any connections between the FRB-host properties and host-burst

offset distributions to those of other astronomical transients such as long-duration GRBs (LGRBs), short-duration GRBs (SGRBs), core-collapse supernovae (CC-SNe), and SNe Ia. Recently, Li & Zhang (2020) and Bhandari et al. (2020b) analyzed a sample of five and six FRB hosts, respectively, and found that their physical properties are most consistent with those of SGRBs and SNe Ia, excluding models in which the majority of FRBs originate from SLSN/LGRB progenitors or active galactic nuclei (AGNs). Here, we leverage our larger sample to further narrow down and provide stronger constraints on the most likely progenitor channels for the majority of FRBs.

We have structured the paper as follows: in Section 2 we define the FRB-host galaxy sample(s) and present the new host-galaxy observations of the ASKAP-localized FRBs characterized here. We detail the modeling of the host-galaxy properties in Section 3 and compare the typical host-galaxy environments to field-selected galaxies in Section 4. In Section 5 we compare the FRBs to other types of astronomical transients and discuss the implications of our results on the most likely FRB progenitor channels. We conclude and summarize our work in Section 6. Throughout the paper, we assume the concordance cosmological model, with $\Omega_m = 0.308$ and $H_0 = 67.8 \text{ km s}^{-1} \text{ Mpc}^{-1}$ (Planck Collaboration et al. 2016).

2. Sample and Observations

In collaboration with the CRAFT (Macquart et al. 2010) and *realfast* (Law et al. 2018) surveys, we have as part of the Fast and Fortunate for FRB Follow-up (F⁴)¹⁸ collaboration endeavored to obtain dedicated photometric and spectroscopic follow-up observations of all \sim arcsecond-localized FRBs. These provide a secure identification of the associated host galaxies and allow us to derive their main physical properties. All the observational data products are available on the FRB GitHub repository,¹⁹ in addition to a large suite of FRB-related scripts. As a front-end to these data repositories, we have also launched an online FRB-host galaxy database,²⁰ with the goal of collecting and sharing all currently known and future FRB hosts and their basic properties.

In this section, we describe the identification of FRB-host galaxies and define a set of sample criteria to describe the robustness of the host associations. We then present the new observations of five FRB-host galaxies and compile all previously known FRB hosts reported in the literature, all considered in our meta analysis. At the end, we summarize the overall sample properties.

2.1. Host-galaxy Associations

An FRB signal alone cannot directly establish the redshift of the source, and one relies on an association with a host galaxy for a precise measurement. To date and in this work, the association of the FRB with a host galaxy is primarily based on probabilistic arguments given their position relative to coincident or nearby galaxies. Following standard practice for other transients (e.g., Bloom et al. 2002; Blanchard et al. 2016, for GRBs), one may estimate the probability of a chance coincidence (P_{chance}) based on the angular offset, θ , of the FRB position from the galaxy centroid, the uncertainty of the FRB

¹⁸ <https://ucolick.org/f-4>

¹⁹ <https://github.com/FRBs/FRB>

²⁰ <https://frbhosts.org>

localization, and the galaxy’s apparent magnitude. Further work may adopt additional properties and priors for establishing associations.

The derivation of P_{chance} is based on galaxy number counts and captures the fact that apparently faint galaxies are more common on the sky. We adopt the formalism developed by Bloom et al. (2002), derived from optical galaxy number counts (Hogg et al. 1997), which gives the number density of galaxies brighter than apparent r -band magnitude m_r (not taking into account clustering of galaxies), as

$$\Sigma(\leq m_r) = \frac{1}{3600^2 \times 0.334 \log_e(10)} \times 10^{0.334(m_r - 22.963) + 4.320} \text{ arcsec}^{-2}. \quad (1)$$

We then calculate the probability of chance coincidence, given by

$$P_{\text{chance}} = 1 - \exp(-\eta), \quad (2)$$

where $\eta \equiv \pi \theta^2 \Sigma(\leq m_r)$. We report the estimated chance probabilities of each of the FRB-host galaxies in Table 1. Here, we also provide the association radius δx , representing the offset from a given galaxy with r -band magnitude m_r within which the FRB can be securely associated with the galaxy (Tunnicliffe et al. 2014).

In previous works, we estimated the probability of chance coincidence with an empirical approach (Bannister et al. 2019) and reported $P_{\text{chance}} < 10^{-3}$ for the first well-localized ASKAP-detected FRBs (e.g., Bannister et al. 2019; Prochaska et al. 2019a). The formalism described above yields consistent results. We note that Eftekhari & Berger (2017) have developed a similar framework to quantify the robustness of the FRB-host galaxy associations with a more recent number count estimation. This generally provides lower chance probabilities; here, we use the formalism described above to be more conservative. In this work, we also estimate the uncertainty on the offsets from the FRB to the host galaxy center by integrating over the FRB localization ellipse.

Our approach is designed to (i) minimize the deleterious effect of false positives on this somewhat small sample of events and (ii) define a high-confidence sample that can be used in future analyses to generate priors for a full Bayesian analysis. To do this, we define four subsamples based solely on P_{chance} and the quality of the galaxy redshift estimation. These are:

1. Sample A: The host-galaxy association is considered highly probable ($P_{\text{chance}} < 0.05$) based on the FRB localization and galaxy photometry. The galaxy has a spectroscopically confirmed redshift z_{spec} .
2. Sample B: Same as Sample A, except that only a photometric redshift z_{phot} has been estimated.
3. Sample C: The host-galaxy association is less secure due to a poor FRB localization, multiple host candidates, and/or because additional priors were adopted in the association (e.g., the Macquart DM- z relation; Macquart et al. 2020). A spectroscopic redshift z_{spec} has been measured.
4. Sample D: Same as Sample C, except that only a photometric redshift z_{phot} has been measured.

We consider all the FRB hosts compiled in this work throughout the paper but caution about the potential pitfalls of

the uncertain host-galaxy identifications where relevant. For the statistical analyses we only consider the FRBs in Sample A. In the following section we introduce all of the candidate FRB-host galaxies and enumerate the number in each sample type.

2.2. FRB-host Galaxy Observations

In continuation of the first four FRBs detected and accurately localized by ASKAP/CRAFT (presented in Bhandari et al. 2020b), we here report the observations and basic properties of five more recent FRB-host galaxies: those of FRBs 190611, 190711, 190714, 191001, and 200430.

2.2.1. FRB 190611

On UT 2019 June 11 at 05:45:43.3, the ASKAP telescope recorded FRB 190611 as reported by Macquart et al. (2020), who also briefly described its host-galaxy candidates. The FRB position is at R.A., decl. (α, δ) = $21^{\text{h}}22^{\text{m}}58^{\text{s}}.91, -79^{\circ}23'51''.3$ (J2000), with an uncertainty of $\sigma_{\alpha, \delta} = 0''.7, 0''.7$.

We obtained deep Gemini-S/GMOS images in the r and i bands (the latter shown in Figure 1) revealing a bright source ($r = 22.65$ mag) approximately $2''$ to the northwest at $\alpha, \delta = 21^{\text{h}}22^{\text{m}}58^{\text{s}}.28, -79^{\circ}23'50''.1$ (J2000), identified as the host galaxy by Macquart et al. (2020). We do not detect any significant structure (e.g., spiral arms) and measure an effective half-light radius of $R_{\text{eff}} = 0''.40$. We also tentatively detect a considerably fainter source coincident within the FRB error ellipse ($r \approx 26$ mag; at $21^{\text{h}}22^{\text{m}}58^{\text{s}}.97, -79^{\circ}23'51''.7$) at a smaller offset of $0''.43$ from the FRB position. We estimate chance probabilities for the two galaxies to be unrelated to the FRB host of $P_{\text{chance}} = 0.017$ and 0.10 for the bright and faint galaxy, respectively. Given the only tentative detection of the faint source and that the bright source has $P_{\text{chance}} \approx 2\%$, we consider the more clearly offset, bright galaxy to be the host of FRB 190611 and place it in our primary Sample A.

Spectroscopy of this host-galaxy candidate with the FORS2 instrument on the ESO Very Large Telescope (VLT) was reduced using the PyPeIt reduction package (Prochaska et al. 2020), which optimally extracts a 1D spectrum from the flat-fielded and sky-subtracted 2D spectral image. We additionally performed a 2D coaddition of the spectra presented in Macquart et al. (2020). This yields a spectroscopic redshift of $z_{\text{spec}} = 0.3778$ based on the H α , H β , and [O III] line features. At this redshift, the physical projected offset of the FRB from the bright galaxy centroid is ≈ 11 kpc.

2.2.2. FRB 190711

On UT 2019 July 11 at 01:53:41.1, the ASKAP telescope recorded FRB 190711 as reported by Macquart et al. (2020), who also provided a brief description of its host galaxy. The FRB position is at $\alpha, \delta = 21^{\text{h}}57^{\text{m}}40^{\text{s}}.68, -80^{\circ}21'28''.8$ (J2000), with an uncertainty of $\sigma_{\alpha, \delta} = 0''.4, 0''.3$ (Day et al. 2020). This FRB has subsequently been found to repeat (Kumar et al. 2020).

The FRB is coincident with an $r \approx 23.5$ mag galaxy at $\alpha, \delta = 21^{\text{h}}57^{\text{m}}40^{\text{s}}.60, -80^{\circ}21'29''.25$ (see Figure 1), with an offset of $0''.49$. No clear morphological structures can be identified in the GMOS imaging, and we measure an effective half-light radius of $R_{\text{eff}} = 0''.46$. We assert a secure association of FRB 190711 to this galaxy, given the low chance probability of $P_{\text{chance}} = 0.011$, and include it in Sample A.

Table 1
Overview of the Main Sample of FRBs and Their Putative Hosts

| FRB | R.A.-FRB (deg) | Decl.-FRB (deg) | σ_R ($''$) | Repeating | R.A.-host (deg) | Decl.-host (deg) | θ ($''$) | δx ($''$) | $r_{1/2}$ ($''$) | r_i ($''$) | m (mag) | Filter | P_{chance} | Sample |
|--------|-------------------|--------------------|------------------------|-----------|--------------------|---------------------|----------------------|------------------------|-----------------------|-------------------|--------------|--------------|---------------------|--------|
| (1) | (2) | (3) | (4) | (5) | (6) | (7) | (8) | (9) | (10) | (11) | (12) | (13) | (14) | (15) |
| 121102 | 82.9946 | 33.1479 | 0.100 | y | 82.9946 | 33.1480 | 0.17 | 1.2 | 0.2 | 0.44 | 23.73 | GMOS_N_r | 0.0023 | A |
| 180916 | 29.5031 | 65.7168 | 0.002 | y | 29.5012 | 65.7147 | 7.87 | 44.8 | 5.1 | 12.95 | 16.17 | SDSS_r | 0.0059 | A |
| 180924 | 326.1052 | -40.9000 | 0.102 | n | 326.1052 | -40.9002 | 0.71 | 4.7 | 0.6 | 1.35 | 20.50 | DES_r | 0.0018 | A |
| 181112 | 327.3485 | -52.9709 | 1.626 | n | 327.3486 | -52.9709 | 0.28 | 2.7 | 1.2 | 3.25 | 21.68 | DES_r | 0.0257 | C |
| 190102 | 322.4157 | -79.4757 | 0.502 | n | 322.4150 | -79.4757 | 0.45 | 4.1 | 1.0 | 2.02 | 20.77 | VLT_FORSS2_I | 0.0050 | A |
| 190523 | 207.0650 | 72.4697 | 2.449 | n | 207.0643 | 72.4708 | 3.79 | 2.4 | 0.5 | 4.90 | 22.01 | Pan-STARRS_r | 0.0733 | C |
| 190608 | 334.0199 | -7.8982 | 0.258 | n | 334.0204 | -7.8989 | 3.00 | 20.5 | 1.3 | 3.96 | 17.55 | SDSS_r | 0.0016 | A |
| 190611 | 320.7455 | -79.3976 | 0.671 | n | 320.7428 | -79.3972 | 2.13 | 2.3 | 0.4 | 2.27 | 22.07 | GMOS_S_r | 0.0169 | A |
| 190614 | 65.0755 | 73.7067 | 0.566 | n | 65.0738 | 73.7064 | 2.22 | 1.4 | 1.0 | 2.99 | 23.25 | GMOS_S_r | 0.0708 | D |
| 190711 | 329.4195 | -80.3580 | 0.350 | y | 329.4192 | -80.3581 | 0.49 | 1.3 | 0.5 | 1.04 | 23.49 | GMOS_S_r | 0.0106 | A |
| 190714 | 183.9797 | -13.0210 | 0.283 | n | 183.9796 | -13.0211 | 0.49 | 4.3 | 1.0 | 2.09 | 20.69 | Pan-STARRS_r | 0.0050 | A |
| 191001 | 323.3516 | -54.7477 | 0.149 | n | 323.3519 | -54.7485 | 2.86 | 13.5 | 1.4 | 4.07 | 18.34 | DES_r | 0.0031 | A |
| 200430 | 229.7064 | 12.3769 | 0.546 | n | 229.7063 | 12.3766 | 1.04 | 3.0 | 0.6 | 1.55 | 21.51 | Pan-STARRS_r | 0.0051 | A |

Note. Column 1: FRB source. Columns 2 and 3: R.A. and decl. of the FRB (J2000). Column 4: Approximate FRB localization uncertainty (geometric mean of R.A. and decl. axes). Column 5: FRB classification. Repeating = yes(y)/no(n). Columns 6 and 7: R.A. and decl. of the associated host galaxy (J2000). Column 8: Projected angular offset of the FRB to the host-galaxy center. Column 9: Association radius δx (Tunnicliffe et al. 2014). Column 10: Angular effective radius of the host measured from a Sérsic model using GALFIT (Peng et al. 2010) on the i -band images (or equivalent). Column 11: Effective search radius (Bloom et al. 2002). Column 12: Measured apparent magnitude of the host. Column 13: Filter used for the magnitude measurement. Column 14: Probability of chance coincidence using the Bloom et al. (2002) formalism. Column 15: Sample designations following the criteria outlined in Section 2.1.

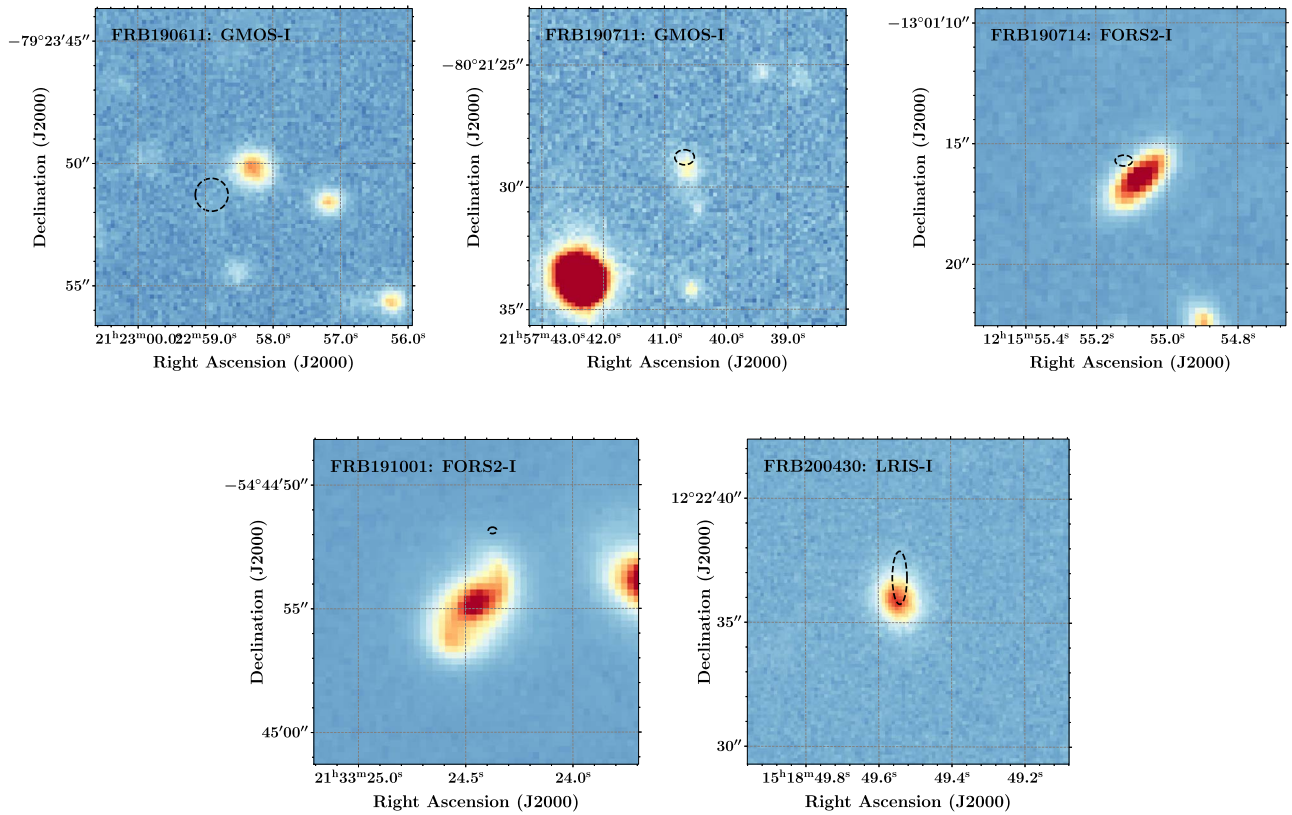


Figure 1. Mosaic showing the *I/i*-band images of the host galaxies of FRBs 190611, 190711, 190714, 191001, and 200430. The dashed black lines represent the total 1σ uncertainties on the FRB positions (statistical and systematic).

Using `PyPeIt`, we have performed a 2D coaddition of the VLT X-Shooter spectra presented in Macquart et al. (2020). Based on the detection of $H\beta$ and $[O\ III]$ in this spectrum, we find $z_{\text{spec}} = 0.5220$. At this redshift, the physical projected offset of the FRB from the galaxy centroid is ≈ 3 kpc. We do not detect $H\alpha$ emission, but this feature lies at a lower throughput portion of the spectrograph where there is also significant telluric absorption.

2.2.3. FRB 190714

On UT 2019 July 14 at 05:37:12.9, the ASKAP telescope recorded FRB 190714 at $\alpha, \delta = 12^{\text{h}}15^{\text{m}}55^{\text{s}}.12, -13^{\text{d}}01^{\text{m}}15^{\text{s}}.7$ (J2000), with an uncertainty of $\sigma_{\alpha,\delta} = 0''.4, 0''.3$. This localization places FRB 190714 $\approx 0''.5$ from the galaxy J121555.0941–130116.004 (see Figure 1), which was previously cataloged by the Pan-STARRS (Chambers et al. 2016) and the VISTA (Cross et al. 2012) surveys. It is a relatively bright source ($r = 20.85$ mag), and we estimate a chance association of $P_{\text{chance}} = 0.005$. We thus include this galaxy in Sample A. We do not detect any distinct morphology of the host galaxy in our FORS2 *I*-band image, but there might be evidence of spiral arms based on preliminary results obtained from imaging with the Hubble Space Telescope (A. Mannings et al. 2020, in preparation). We measure an effective half-light radius of $R_{\text{eff}} = 1''.02$.

We obtained optical spectroscopy of the host of FRB 190714 on 2020 January 28 with the LRIS spectrometer (Oke et al. 1995) on the Keck I 10 m telescope. This dual-camera instrument was configured with the 600/7500 grating, the 600/4000 grism, and a slit mask designed to observe the FRB-host and additional galaxies in the field. We reduced these data

with `PyPeIt`, and the extracted 1D spectrum was then flux-calibrated through observations of a spectroscopic photometric standard acquired on the same (clear) night and scaled to the Pan-STARRS photometry. The bright nebular emission lines of $H\beta$, $[O\ III]$, $H\alpha$, and $[N\ II]$ yield a spectroscopic redshift of $z_{\text{spec}} = 0.2365$. This places FRB 190714 at a projected physical separation of ≈ 2 kpc from the galaxy center.

2.2.4. FRB 191001

On UT 2019 October 01 at 16:55:36.0, the ASKAP telescope recorded FRB 191001 at $\alpha, \delta = 21^{\text{h}}33^{\text{m}}24^{\text{s}}.373, -54^{\text{d}}44^{\text{m}}51^{\text{s}}.4$ (J2000), with an uncertainty of $\sigma_{\alpha,\delta} = 0''.17, 0''.13$ (Bhandari et al. 2020a). This position is $\approx 2''.9$ north of the previously cataloged source DESJ213324.44–544454.65 (Figure 1; Abbott et al. 2018). Despite the relatively large angular offset, the bright magnitude ($r = 18.41$ mag) yields a chance coincidence probability of only $P_{\text{chance}} = 0.003$. We therefore include this galaxy in Sample A. The host galaxy of this FRB shows clear spiral-arm features, with the FRB occurring in the outskirts of the northern arm (see Bhandari et al. 2020a, for a more detailed study of this FRB). The estimated effective half-light radius is $R_{\text{eff}} = 1''.44$.

On UT 2019 October 4, we obtained a GMOS spectrum of the host of FRB 191001 with the Gemini-S telescope, configured with a $1''$ long slit and the R400 grating tilted to cover $\lambda \approx 5000\text{--}9900\text{ \AA}$ with a full width at half maximum (FWHM) $\approx 500\text{ km s}^{-1}$. The data were reduced with the `PyPeIt` software package (see Section 2.2.1 for details) and flux calibrated with a standard star obtained and scaled to $r = 18.4$ mag. The detection of strong nebular emission lines from $H\beta$, $[O\ III]$, $H\alpha$, and $[N\ II]$ yield a spectroscopic redshift

of $z_{\text{spec}} = 0.2340$. This places FRB 191001 at a projected physical separation of ≈ 11 kpc from the galaxy center.

The longslit was oriented at $\text{PA} = 100^\circ$ to include the neighboring galaxy J213323.65–544453.6, which lies $\approx 7''$ east of the identified host galaxy. Its spectrum also shows strong nebular emission yielding $z_{\text{spec}} = 0.2339$, i.e., coincident with the host of FRB 191001, revealing a physical pair. At a projected separation of ≈ 25 kpc, we expect that these galaxies are in the process of merging.

2.2.5. FRB 200430

On UT 2020 April 30 at 15:49:48.3, the ASKAP telescope recorded FRB 200430 at $\alpha, \delta = 15^{\text{h}}18^{\text{m}}49^{\text{s}}.54, +12^{\circ}22^{\text{m}}36^{\text{s}}.8$ (J2000), with an uncertainty of $\sigma_{\alpha, \delta} = 0''.3, 1''.1$. This is $\approx 1''.0$ north of the previously cataloged galaxy J151849.52 +122235.82 in the Pan-STARRS catalog (Chambers et al. 2016) with $r = 21.51$ mag. We obtained additional g - and i -band imaging with Keck/LRIS on UT 2020 June 21, the latter shown in Figure 1. Based on the offset and the host-galaxy magnitude, we derive a chance coincidence probability of $P_{\text{chance}} = 0.005$. We therefore include this galaxy in Sample A. We do not detect any distinct morphology of the host galaxy based on the deeper Keck images and measure an effective half-light radius of $R_{\text{eff}} = 0''.57$.

On UT 2020 May 16, we obtained optical spectroscopy of the identified host galaxy with the Alhambra Faint Object Spectrograph and Camera (ALFOSC) mounted at the Nordic Optical Telescope (NOT). The spectra were obtained with grism 4 (covering 3200–9600 Å) and a slit width of $1''.3$. The observations were performed under good conditions with an average seeing of $1''.1$ at an airmass around 1.2 during the integration. The data were reduced with the `PyPeIt` software package. We determine a redshift for the host galaxy of $z = 0.161$ based on the detection of the $\text{H}\alpha$, $[\text{O II}]$, and $[\text{S II}]$ emission features and the H and K absorption lines from Ca. This places FRB 200430 at a projected physical separation of ≈ 3 kpc from the galaxy center.

2.3. Literature Compilation

In addition to the five new FRB hosts presented here, we include all other (currently) known FRB-host galaxies in our analysis. These include FRBs 121102 (Bassa et al. 2017; Chatterjee et al. 2017; Tendulkar et al. 2017), 180916 (Marcote et al. 2020), 180924 (Bannister et al. 2019; Bhandari et al. 2020b), 181112 (Prochaska et al. 2019a), 190102 (Bhandari et al. 2020b; Macquart et al. 2020), 190523 (Ravi et al. 2019), 190608 (Bhandari et al. 2020b; Chittidi et al. 2020; Macquart et al. 2020), and 20190614D (hereafter referred to as FRB 190614; Law et al. 2020).

In Appendix A we briefly describe these additional galaxies associated with well-localized FRBs and any new observations obtained after the primary publications. We separate them primarily by FRB survey. For the hosts previously reported by Bhandari et al. (2020b), we simply include their reported measurements here. For the host galaxy of FRB 180916 (Marcote et al. 2020), we extract the photometry from the SDSS and Wide-field Infrared Survey Explorer (WISE) catalogs to obtain a more precise estimate of the stellar mass. We find the best-fit value to be approximately a factor of five lower than the stellar mass reported by Marcote et al. (2020). We also obtained independent spectra of the putative host

galaxy of FRB 190523 (Prochaska et al. 2019b; Ravi et al. 2019), allowing us to derive an upper limit on the line flux of $\text{H}\beta$, which we use to place a stronger limit on the star-formation rate (SFR) of $< 0.09 M_\odot \text{ yr}^{-1}$. Finally, we used the photometry reported by Bassa et al. (2017) for the host galaxy of FRB 121102 to model our own spectral energy distribution (SED; see Section 3.1) for consistency with the rest of the sample.

2.4. Overall Sample Properties

Our overall parent sample consists of 13 FRB-host galaxies as presented in Table 1. Out of these 13 hosts, 10 satisfy the Sample A criteria. These include all the 5 new host galaxies characterized in detailed here (FRBs 190611, 190711, 190714, 191001, and 200430) and the hosts of FRBs 121102, 180916, 180924, 190102, and 190608 (i.e., all the hosts of the repeating FRBs are also in Sample A). We have placed the host of FRB 190523 discovered by Ravi et al. (2019) into Sample C because the poor FRB localization makes the host-galaxy association less secure. The host galaxy of FRB 181112 identified by Prochaska et al. (2019a) is also placed in Sample C because the proposed foreground galaxy has a similarly low ($P_{\text{chance}} < 0.05$) chance association probability. The observed dispersion measure of $\text{DM}_{\text{FRB}} = 589 \text{ pc cm}^{-3}$ for this event, however, supports the association that the background galaxy is the host of FRB 181112. To be conservative and consistent with the other sample classifications, we rely only on the statistical properties of the FRB-host associations here to avoid biasing the host identifications. For FRB 190614, Law et al. (2020) identified two potential host-galaxy candidates, for which only photometric redshifts have been obtained, placing it in Sample D.

This more than doubles the number of ASKAP-detected FRB hosts studied in our previous work (Bhandari et al. 2020b). The FRBs are distributed throughout the celestial sphere, and our full sample spans redshifts of $z_{\text{FRB}} = 0.03\text{--}0.66$. We wish to caution, however, that because the number of FRB-host identifications is still small, we consider all known FRB hosts here regardless of their initial selection. A more careful homogeneous selection is required when a larger number of FRBs with subarcsecond localizations and their associated host galaxies have been properly identified.

2.5. Repeating and Nonrepeating FRBs

Throughout the paper, we distinguish the hosts of the three FRBs that are currently known to repeat (FRBs 121102, 180916, and 190711) from the hosts of the other apparently nonrepeating one-off FRBs. Repeating FRBs by definition cannot be cataclysmic events, whereas apparently nonrepeating FRBs might be. In principle, all FRBs could be found to repeat if observed on long enough timescales and with an appropriate cadence, but it appears unlikely that they do (at least similarly to FRB 121102; James et al. 2020). The apparently longer intrinsic temporal pulse width for repeating FRBs compared as an ensemble to as yet nonrepeating FRBs (CHIME/FRB Collaboration et al. 2019; Fonseca et al. 2020) also suggests that repeating sources show different pulse morphologies than nonrepeating sources, including wider burst envelopes and distinct time-frequency drifting. This could imply a different emission mechanism for repeating and one-off sources. We caution that it is possible that FRBs that are currently classified as nonrepeating may exhibit repeat pulses in

the future, which would change their classification here. As noted by Day et al. (2020) and others, signposts of probable repetition can be discerned from high time and frequency resolution analyses of FRB detections, although it appears to reflect a continuum of spectro-temporal polarimetric properties of FRBs more. Here, we reserve the repeater label for events with multiple confirmed bursts.

Even with a sample of three known repeating FRBs, it is possible to examine the physical properties of their host galaxies compared to the sample of hosts of apparently nonrepeating FRBs. This may provide additional clues on whether two populations of FRBs exist.

3. Analysis and Results

3.1. Stellar Population Modeling

Following our previous studies of FRB-host galaxies (Bannister et al. 2019; Prochaska et al. 2019a; Bhandari et al. 2020b; Chittidi et al. 2020), we have analyzed the existing photometry and spectroscopy of all hosts with the `pPXF` (Cappellari 2017) and `CIGALE` (Noll et al. 2009) software packages. Each package fits a set of stellar population models and a star formation history (SFH) to the spectra (`pPXF`) or photometry (`CIGALE`) and generates best estimates for quantities such as stellar mass M_* , internal extinction $E(B - V)$, and age of the main stellar population.

We adopt the following assumptions in these analyses:

1. A delayed-exponential SFH model with no late-burst population ($\text{SFR}(t) \propto t/\tau^2 \times \exp(-t/\tau)$). Here t is the age, with $t = 0$ the onset of star formation, and τ is the e -folding time of the decaying part of the SFH.
2. The Bruzual & Charlot (2003) simple stellar population with the initial mass function (IMF) from Chabrier (2003) and a metallicity allowed to vary from $0.005Z_\odot$ to $2.55Z_\odot$.
3. The Calzetti et al. (2000) dust extinction model, modified following Lo Faro et al. (2017).
4. The Dale et al. (2014) dust emission model with an AGN fraction $f_{\text{AGN}} \leq 0.2$ and a power-law exponent of 2.

We determine the internal host-galaxy extinction $E(B - V)_{\text{host}}$ from the SED modeling without adopting the visual extinction derived from the Balmer decrement as input, but note that the two independent estimates are generally consistent. In all cases, we have input observations corrected for Galactic extinction using the $E(B - V)_{\text{Gal}}$ values derived from Schlafly & Finkbeiner (2011) and the Fitzpatrick & Massa (2007) extinction law with $R_V = 3.1$ implemented in the `extinction`²¹ software package. The derived photometry for all FRB hosts considered here is provided in Appendix B, in Tables 6–8. The precise input parameter file for `CIGALE` is available in the `cigale.py` module of the FRB repository on GitHub.

The best-fit models for the host galaxies described in Section 2.2 are presented in Figures 2 and 3. These include fluxes for common emission lines derived from the `pPXF` analysis (provided in Table 2), which corrects for Balmer absorption. For uniformity, we also performed the same analysis on FRB hosts drawn from the literature, especially for all galaxies in Sample A. This includes reanalyses of hosts from our own previous publications (e.g., Bhandari et al. 2020b). Any

substantial differences from previously reported estimates are described in Appendix A. The results are summarized in Table 3.

3.2. Star Formation Rate

We derive the SFR for each FRB host by first computing the dust-corrected $\text{H}\alpha$ line fluxes using the A_V derived from the Balmer decrement to obtain the intrinsic $\text{H}\alpha$ line luminosities as $L_{\text{H}\alpha} (\text{erg s}^{-1}) = F_{\text{H}\alpha} (\text{erg s}^{-1} \text{cm}^{-2}) \times 10^{A(\lambda)/2.5} \times (4\pi d_L^2)$, with d_L the luminosity distance.

This we translate into an SFR via the conversion factor

$$\text{SFR}(M_\odot \text{ yr}^{-1}) = 4.98 \times 10^{-42} L_{\text{H}\alpha} (\text{erg s}^{-1}) \quad (3)$$

following Kennicutt (1998), but adopting the IMF from Chabrier (2003).²² We report the uncertainties on the SFR estimates including the scatter in the $\text{SFR}-L_{\text{H}\alpha}$ relation ($\approx 30\%$). For the three FRB hosts where the $\text{H}\alpha$ line flux has not been measured, we derive the SFR from $\text{H}\beta$ assuming the nominal relative strength compared to $\text{H}\alpha$ (FRB190523 in Sample C and FRB190711 in Sample A) or from the best-fit SED model from `CIGALE` (for FRB 200430, Sample A). We find that the overall sample of FRB hosts are characterized by a large range in SFR, spanning $0.05\text{--}10 M_\odot \text{ yr}^{-1}$. For the host of FRB 190614, no constraints could be placed on the SFR because the nature of the host galaxy and redshift are uncertain (Sample D; Law et al. 2020).

3.3. Gas-phase Metallicity

To infer the gas-phase metallicities of the FRB hosts, we rely on commonly used diagnostic ratios of strong nebular emission lines (see Maiolino & Mannucci 2019, for a recent review). These allow us to compute the oxygen abundances $12 + \log(\text{O}/\text{H})$ for each host galaxy. The strong-line diagnostics are calibrated to more direct methods, relying on measurements of the electron temperature T_e or derived from photoionization models. In the following, we adopt the O3N2 calibration from Hirschauer et al. (2018), which parameterizes the oxygen abundance as

$$12 + \log(\text{O}/\text{H}) = 8.987 - 0.297 \times \text{O3N2} - 0.0592 \times \text{O3N2}^2 - 0.0090 \times \text{O3N2}^3, \quad (4)$$

where $\text{O3N2} = \log([(\text{O III})\lambda 5007/\text{H}\beta]/[(\text{N II})\lambda 6584/\text{H}\alpha])$. This calibration has been shown to be consistent with more direct T_e -based methods, and has an rms uncertainty of 0.111 dex. The majority of the FRB hosts are relatively metal rich, with oxygen abundances distributed between $12 + \log(\text{O}/\text{H}) = 8.7\text{--}9.0$. For the host of FRB 121102, we could only place an upper limit on the oxygen abundance of $12 + \log(\text{O}/\text{H}) < 8.08$ because of the non-detection of $[\text{N II}]\lambda 6584$. For the hosts of FRBs 190523, 190614, 190711, and 200430, too few nebular lines have been detected to determine their metallicity.

We caution that because the oxygen abundances derived using the O3N2 calibration are specifically calibrated to SF galaxies, the actual metallicities might be slightly different if the emission-line ratios do not represent typical SF galaxies (as reported for FRB hosts by Bhandari et al. 2020b, see also Section 4.2). However, because the adopted calibration takes

²¹ <https://extinction.readthedocs.io/en/latest>

²² Assuming a conversion from the Salpeter-determined SFR of $\text{SFR}_{\text{Chab}} = \text{SFR}_{\text{Salp}} \times 0.63$.

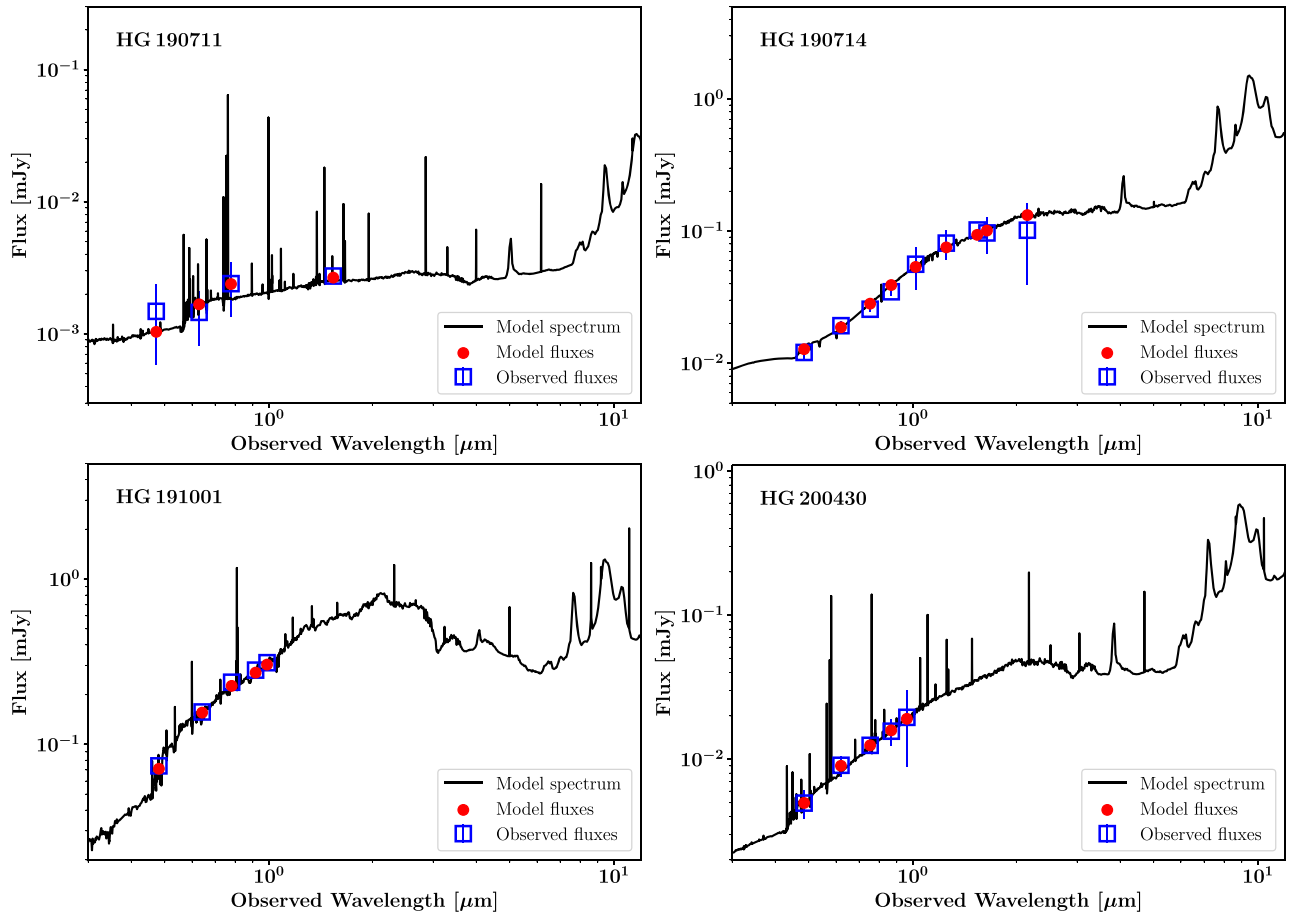


Figure 2. SED models for the host galaxies of FRBs 190711, 190714, 191001, and 200430 (named with an HG prefix). FRB 190611 is not shown here because we do not have sufficient photometric data to construct the SED of the host. The best-fit SED models from CIGALE are shown as solid black lines, the observed magnitudes (corrected for Galactic extinction and converted into fluxes) as blue squares, and the model fluxes as red dots. In all models, the redshift has been fixed to z_{spec} .

both the $[\text{N II}]/\text{H}\alpha$ and the $[\text{O III}]/\text{H}\beta$ ratios into account, the line flux excess of the two ratios should effectively cancel out.

4. Physical Properties of the FRB-host Population

The physical properties of all the FRB hosts in our sample are summarized in Table 3. In the following analysis, we examine the FRB-host galaxy environments and place them into context of field-selected galaxies. Throughout, we separate the hosts of repeating and seemingly nonrepeating, one-off FRBs. We only consider the 10 FRB hosts in Sample A for the statistical analyses.

4.1. Luminosity and Color

To place the FRB hosts in the context of galaxies at similar redshifts, we present the apparent r -band magnitudes m_r of the FRB hosts as a function of redshift in Figure 4. We compare the values of m_r to the characteristic luminosity L^* across redshift, using available galaxy luminosity functions (Brown et al. 2001; Wolf et al. 2003; Willmer et al. 2006; Reddy & Steidel 2009; Finkelstein et al. 2015). For each redshift, we adopt the value of L^* in the rest-frame band that corresponds to the observed r band. Interpolation across redshift results in smooth contours corresponding to the luminosity tracks of field-selected galaxies at $L = 0.01L^*$, $0.1L^*$, and L^* . We find that the majority of the FRB hosts are in the intermediate region

between $L \sim 0.1L^* - L^*$ compared to the underlying galaxy population at $0.0 < z < 0.7$. The only exception is the host galaxy of FRB 121102 (Tendulkar et al. 2017), which has a luminosity of $L \sim 0.01L^*$.

We then consider the color–magnitude properties of the FRB hosts, which is a useful indicator of the overall stellar population in these galaxies. In Figure 5 we compare the absolute r -band magnitudes M_r and the rest-frame $M_u - M_r$ colors of the FRB hosts to the galaxies from the PRIMUS survey (Moustakas et al. 2013), here representing the general population of $z < 0.5$ galaxies. We find that the majority of FRB-host galaxies sample the brighter region of the magnitude distribution, consistent with the initial sample studied in Bhandari et al. (2020b). This suggests that FRB hosts typically trace more massive galaxies than the underlying galaxy population (see also Section 4.3). Moreover, we note that the host galaxies of the three repeating FRBs are fainter than nearly all of the hosts of the apparently nonrepeating FRBs.

Approximately half of the FRB-host galaxies have colors consistent with the SF so-called “blue cloud,” similar to most late-type galaxies (Strateva et al. 2001). The remainder (FRBs 180916, 180924, 190523, 191001, and 200430) are located in the so-called “green valley,” the intermediate region between the two main populations. These galaxies may be transitioning from SF to the quiescent galaxies of the “red sequence” (Martin et al. 2007).

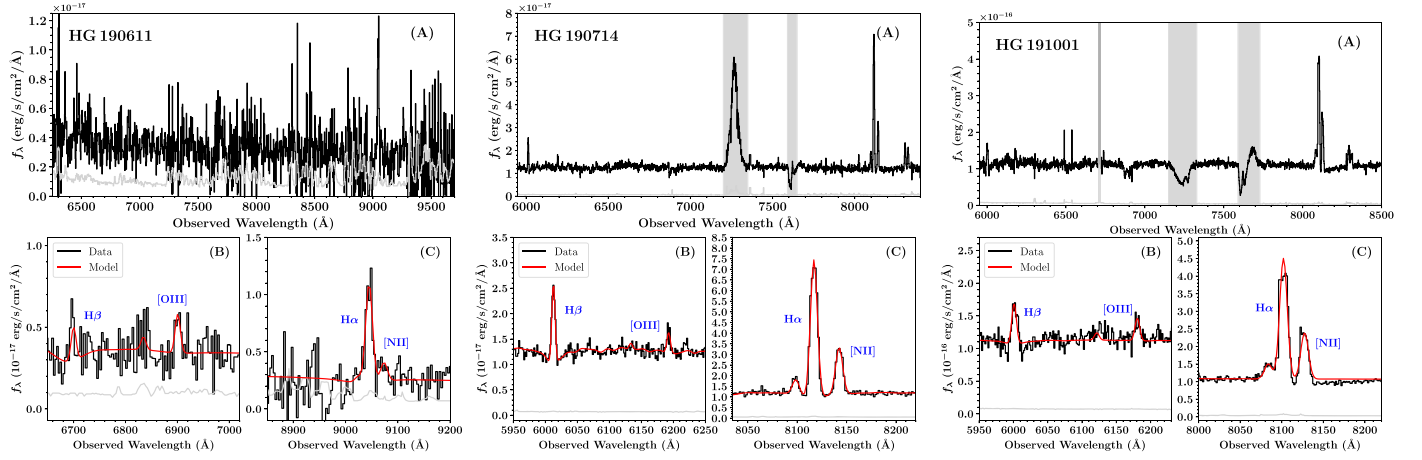


Figure 3. Spectra of the host galaxies of FRBs 190611, 190714, and 191001 (named with an HG prefix). FRBs 190711 and 200430 are not shown here because the poor signal-to-noise ratio (S/N) of the spectra does not allow us to model the line features with pPXF. The solid black lines show the dust-corrected spectra, with the associated error spectrum shown in gray. In the bottom panels, we show zoom-ins on the most prominent nebular emission lines from H α , H β , [O III], and [N II], with the best-fit models from pPXF overplotted on the spectra shown as solid red lines. Strong telluric regions are masked out by the gray shaded regions.

Table 2
Nebular Emission-line Fluxes

| FRB host | H α | H β | [O II] | | [O III] | | [N II] |
|----------|-----------------|-----------------|-----------------|-----------------|-----------------|-----------------|-----------------|
| | | | $\lambda 3726$ | $\lambda 3729$ | $\lambda 4959$ | $\lambda 5007$ | $\lambda 6584$ |
| 121102 | 2.61 ± 0.04 | 0.96 ± 0.09 | ... | ... | ... | 4.38 ± 0.08 | <0.12 |
| 180916 | 40.3 ± 0.2 | ... | ... | ... | 5.91 ± 0.62 | 71.6 ± 0.6 | 15.2 ± 0.2 |
| 180924 | 2.79 ± 0.03 | 0.72 ± 0.02 | 0.40 ± 0.02 | 0.69 ± 0.03 | ... | 0.79 ± 0.02 | 1.94 ± 0.03 |
| 181112 | 0.64 ± 0.30 | 0.29 ± 0.02 | ... | ... | ... | 0.54 ± 0.03 | 0.49 ± 0.30 |
| 190102 | 5.66 ± 0.17 | 1.90 ± 0.17 | 3.20 ± 0.28 | 4.21 ± 0.30 | ... | 3.80 ± 0.27 | 1.69 ± 0.19 |
| 190523 | ... | <0.03 | ... | ... | ... | ... | ... |
| 190608 | 27.7 ± 0.4 | 8.37 ± 0.33 | 12.1 ± 0.7 | 19.4 ± 0.8 | ... | 15.0 ± 0.4 | 18.3 ± 0.4 |
| 190611 | 0.49 ± 0.05 | 0.12 ± 0.03 | ... | ... | ... | 0.18 ± 0.04 | 0.12 ± 0.04 |
| 190711 | ... | 0.26 ± 0.05 | ... | ... | ... | ... | ... |
| 190714 | 3.89 ± 0.03 | 0.97 ± 0.03 | ... | ... | ... | 0.31 ± 0.03 | 1.70 ± 0.03 |
| 191001 | 27.4 ± 0.3 | 5.01 ± 0.30 | ... | ... | ... | 3.62 ± 0.35 | 13.9 ± 0.2 |
| 200430 | ... | ... | ... | ... | ... | ... | ... |

Note. Measurements are in units of $10^{-16} \text{ erg s}^{-1} \text{ cm}^{-2}$ and corrected for Galactic dust using the $E(B - V)$ values derived from Schlafly & Finkbeiner (2011).

Figure 5 further reveals that the FRB hosts do not populate either of the main loci of the blue or red sequences. To quantify this impression, we perform 2D Kolmogorov–Smirnov (KS) tests on the color–magnitude distribution of FRB-host galaxies (considering one-off, repeaters, and the full population) compared to the distribution of early- and late-type galaxies. The results are summarized in Table 4. The hypothesis that the full FRB population is drawn from the same underlying distribution as the full galaxy population is rejected with a KS probability $P_{\text{KS}} = 0.007$. Other scenarios are rejected at higher significance levels ($P_{\text{KS}} < 0.002$). Considering only the repeating FRBs, we find P_{KS} values consistent with those drawn from the late-type population.

4.2. FRB Hosts in the BPT Diagram

In Figure 6 we show the [O III]/H β and [N II]/H α nebular emission-line ratios of the FRB hosts in a Baldwin–Phillips–Terlevich (BPT) diagram (Baldwin et al. 1981). This allows us to assess the dominant source of ionization and distinguish between typical SF galaxies, low-ionization nuclear emission-line region (LINER) galaxies, and AGNs (see Kewley et al. 2019, for a recent review).

We have measured emission-line fluxes for the majority of the hosts in Sample A, most of which were previously reported in Bhandari et al. (2020b). For comparison, we show the distribution of $\sim 75,000$ nearby ($0.02 < z < 0.4$) emission-line galaxies from the Sloan Digital Sky Survey (SDSS), with each emission line required to be detected at $S/N > 5$. We also include the standard demarcation lines between SF, AGN, and LINER galaxies (Kauffmann et al. 2003; Cid Fernandes et al. 2010).

Examining Figure 6, we find that the FRB hosts occupy a distinct region of the BPT diagram from the dominant locus of SF galaxies: the majority of FRB hosts show an excess in the [N II]/H α ratio compared to the ridge line tracing the highest density of local SF galaxies (Brinchmann et al. 2008), with many located in the LINER region. The only exception is the host galaxy of the repeater FRB 121102, which is located in the tail of the SF galaxy population.

We use 2D KS tests to compare the FRB-host galaxy population (both with and without the repeater FRB 121102) to each galaxy class. Galaxy classes are assigned according to the BPT diagram (Figure 6), and the results are summarized in Table 5. The FRB-host galaxy population is statistically

Table 3
Host-galaxy Properties

| FRB host | z_{host} | M_r (mag) | $M_u - M_r$ (mag) | M_* ($10^9 M_\odot$) | SFR ($M_\odot \text{ yr}^{-1}$) | Age (Gyr) | Z $12 + \log(\text{O}/\text{H})$ | Offset (kpc) | R_{eff} (kpc) |
|----------|-------------------|-------------------|----------------------|-----------------------------|--------------------------------------|--------------|---------------------------------------|-----------------|---------------------------|
| (1) | (2) | (3) | (4) | (5) | (6) | (7) | (8) | (9) | (10) |
| 121102 | 0.1927 | -16.20 ± 0.08 | 1.49 ± 0.18 | 0.14 ± 0.07 | 0.15 ± 0.04 | 0.26 | < 8.08 | 0.6 ± 0.3 | 0.7 ± 0.1 |
| 180916 | 0.0337 | -19.46 ± 0.05 | 1.53 ± 0.06 | 2.15 ± 0.33 | 0.06 ± 0.02 | 0.15 | ... | 5.5 ± 0.1 | 3.6 ± 0.4 |
| 180924 | 0.3212 | -20.81 ± 0.05 | 1.78 ± 0.15 | 13.2 ± 5.1 | 0.88 ± 0.26 | 0.38 | $8.93^{+0.02}_{-0.02}$ | 3.4 ± 0.5 | 2.7 ± 0.1 |
| 181112 | 0.4755 | -20.40 ± 0.07 | 1.12 ± 0.15 | 3.98 ± 2.02 | 0.37 ± 0.11 | 0.57 | $8.86^{+0.10}_{-0.13}$ | 1.7 ± 19.2 | 7.2 ± 1.7 |
| 190102 | 0.2912 | -19.85 ± 0.06 | 1.40 ± 0.12 | 3.39 ± 1.02 | 0.86 ± 0.26 | 0.06 | $8.70^{+0.07}_{-0.08}$ | 2.0 ± 2.2 | 4.4 ± 0.5 |
| 190523 | 0.6600 | -22.06 ± 0.12 | 1.92 ± 0.19 | 61.2 ± 40.1 | $< 0.09^a$ | 0.69 | ... | 27 ± 23 | 3.3 ± 0.2 |
| 190608 | 0.1178 | -21.22 ± 0.05 | 1.40 ± 0.09 | 11.6 ± 2.8 | 0.69 ± 0.21 | 0.38 | $8.85^{+0.02}_{-0.02}$ | 6.6 ± 0.6 | 2.8 ± 0.2 |
| 190611 | 0.3778 | ... | ... | ~ 0.8 | 0.27 ± 0.08 | ... | $8.71^{+0.17}_{-0.28}$ | 11 ± 4 | 2.1 ± 0.1 |
| 190711 | 0.5220 | -19.01 ± 0.08 | 0.95 ± 0.16 | 0.81 ± 0.29 | 0.42 ± 0.12^a | 0.61 | ... | 3.2 ± 2.1 | 2.9 ± 0.2 |
| 190714 | 0.2365 | -19.92 ± 0.05 | 1.19 ± 0.17 | 14.9 ± 7.1 | 0.65 ± 0.20 | 1.59 | $9.03^{+0.04}_{-0.04}$ | 1.9 ± 1.1 | 3.9 ± 0.1 |
| 191001 | 0.2340 | -22.13 ± 0.05 | 1.67 ± 0.19 | 46.4 ± 18.8 | 8.06 ± 2.42 | 0.64 | $8.94^{+0.05}_{-0.05}$ | 11 ± 1 | 5.5 ± 0.1 |
| 200430 | 0.1600 | -18.05 ± 0.05 | 1.78 ± 0.31 | 1.30 ± 0.60 | $\sim 0.2^b$ | 0.69 | ... | 3.0 ± 2.4 | 1.6 ± 0.5 |

Notes. Column 1: FRB source. Column 2: Host redshift. Spectroscopic redshifts are reported to four significant digits (typical uncertainty), and photometric redshifts to two significant digits. Column 3: Absolute r -band magnitude. Column 4: Rest-frame $M_u - M_r$ colors. Column 5: Stellar mass from SED modeling. Column 6: Star-formation rate derived from the line luminosity of $\text{H}\alpha$, assuming a Chabrier (2003) IMF. Column 7: Estimate of the mass-weighted stellar population age from SED modeling. Column 8: Oxygen abundance derived using the O3N2 calibration from Hirschauer et al. (2018). Column 9: Projected physical offset of the FRB from the galaxy center. Column 10: Effective radius of the host galaxy measured in the i band (or equivalent).

^a The SFR is derived from $\text{H}\beta$ assuming a nominal scaling with $\text{H}\alpha$ (i.e., no internal host extinction).

^b The SFR is derived from the best-fit photometric SED model.

inconsistent with the distribution of SF galaxies ($P_{\text{KS}} = 0.015$) and may favor the AGN+LINER populations.

The excess of emission-line ratios from the locus of regular SF galaxies in the BPT diagram is generally attributed to a hard stellar ionizing radiation field or elevated ionization parameters of the interstellar medium (ISM; Brinchmann et al. 2008; Steidel et al. 2014). The underlying emission mechanism is not completely clear, however. Thomas et al. (2018) argue that the excess in line flux ratios can be described by an increased “mixing” of AGN emission with the H II region emission. Alternatively, the same ionization effect can be produced by a dominating population of post-asymptotic giant branch (post-AGB) stars (Yan & Blanton 2012; Singh et al. 2013). The latter scenario aligns with the typical old stellar populations of the FRB hosts inferred from the SED modeling (see Section 3.1 and Table 3). We do note, however, that the host galaxy of FRB 190608 is found to contain a Type I AGN based on the detection of broad $\text{H}\alpha$ emission (Stern & Laor 2012; Chittidi et al. 2020). We do not detect similar broad $\text{H}\alpha$ emission lines in the other FRB-host spectra. Ultimately, integral field unit (IFU) observations at high spatial resolution of the host galaxies are needed to distinguish whether the central AGN or the overall LINER emission are the most common emission mechanisms producing the elevated ionization observed in FRB hosts.

4.3. Star Formation Rates and Stellar Masses

We show the SFR– M_* distribution of the FRB hosts in Figure 7. For the control sample, we again show the galaxies from the PRIMUS survey (Moustakas et al. 2013). We caution that due to the LINER-like emission observed for most of the FRB-host galaxies, the SFR could in some cases only represent an upper limit on the actual rate because the total line emission might not solely reflect the star formation activity.

Similar to the color–magnitude distribution (Figure 5; Section 4.1), we find that the FRB-host galaxies avoid the

main sequence of SF galaxies (i.e., the main locus of the control sample). Moreover, a 2D KS test yields a low probability that the two distributions were drawn from the same parent population ($P_{\text{KS}} < 0.001$). Intriguingly, the host galaxies of the known repeating FRBs show more diverse behavior than those hosting nonrepeating bursts, ranging from faint starburst (FRB 121102), to regularly SF (FRB 190711), and finally to quiescent (FRB 180916) galaxies. The hosts of the repeating FRBs are all relatively low-mass galaxies ($M_* < 2 \times 10^9 M_\odot$) compared to the overall FRB-host population (as described before in Section 4.1).

We now consider the hypothesis that FRBs track stellar mass. Specifically, we compare the observed distribution $f_{\text{FRB}}(M_*)$ with the stellar mass function of low- z galaxies $\phi(M_*)$ weighted by stellar mass, i.e., $f_{\text{FRB}}(M_*) \propto M_* \phi(M_*)$. For this analysis we assume the parameterization of $\phi(M_*)$ derived by Davidzon et al. (2017) for galaxies at $0.2 < z < 0.5$ in the COSMOS field.

In Figure 8 we plot the cumulative stellar mass distribution of the FRB hosts in Sample A. We first consider all the hosts (top panel) and then only the hosts of the one-off FRBs (bottom panel). The uncertainty regions on the cumulative distribution functions (CDFs) are estimated by combining the two sources of uncertainty: the errors on the individual data points, and the error from the sample size. We calculate the former using Monte Carlo error propagation, assuming that the probability density function (PDF) of each data point is described by a Gaussian profile, with the standard deviation given by the error on the measurement (similar to the procedure described in Palmerio et al. 2019). We then estimate the median and 1σ confidence bounds on the CDF from 10,000 realizations of the data sampling. The error from the sample size is then computed via bootstrapping and added to show the combined uncertainty region.

A comparison of the CDF of all the FRB hosts to the mass-weighted stellar mass distribution of field galaxies $f_{\text{FRB}}(M_*)$

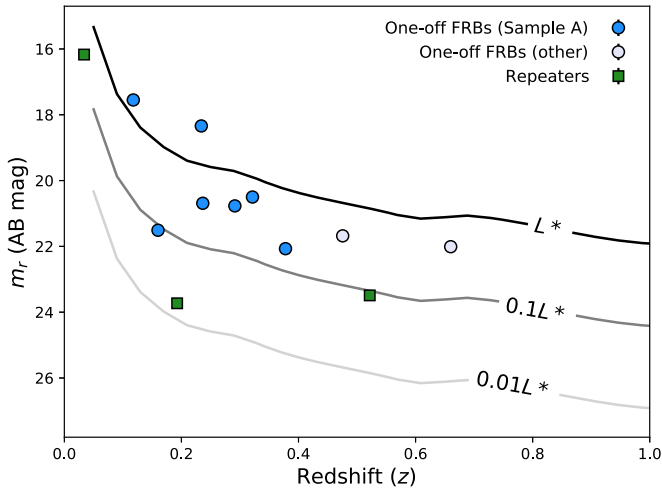


Figure 4. Observed apparent r -band magnitude as a function of redshift for the host galaxies of repeating and nonrepeating FRBs. The nonrepeating FRBs are marked by blue (Sample A) and gray (other samples) dots, and repeating FRBs (all in Sample A) are denoted by green squares. For FRB 190102 we plot the i -band magnitude, since the r -band is not available. For comparison, we show constant luminosity tracks of the underlying field galaxy population at $L = 0.01L^*$, $0.1L^*$, and L^* , which were constructed using the appropriate rest-frame band galaxy luminosity function that corresponds to the observed r band at each redshift. All FRB hosts are luminous with $L > 0.1L^*$, except for that of the repeater, FRB 121102, which has a luminosity of $L < 0.01L^*$.

yields a probability of $P_{KS} < 0.001$ from a one-sided KS test for the two distributions to be drawn from the same underlying mass distribution. Therefore these results rule out the null hypothesis that FRBs directly track stellar mass. When we limit this to one-off FRBs (Figure 8, lower panel) the offset is reduced, but the probability remains low.

4.4. Mass–Metallicity Relation

In addition to the stellar mass and SFR, the gas-phase metallicity is a strong indicator of the present stellar populations and can thus also provide constraints on the most likely progenitor channels. Indeed, the typical low-metallicity environments of LGRB host galaxies were vital in the conception of the “collapsar” progenitor model for LGRBs (e.g., Yoon et al. 2006). A more direct, quantitative comparison between FRB and LGRB hosts (in addition to the hosts of other types of transients) is provided in Section 5.1.

In Figure 9 we show the metallicities of the FRB-host galaxies in terms of their oxygen abundances $12 + \log(\text{O}/\text{H})$ as a function of stellar mass (i.e., the mass–metallicity relation). For the control sample, we show the SF galaxies from the SDSS emission-line sample, with metallicities calibrated using the same strong-line diagnostics as for the FRB hosts (see Section 3.3). For comparison, we overplot the mass–metallicity relations at $z \sim 0.07$ and $z \sim 0.7$ by Maiolino et al. (2008). We find that the majority of FRB hosts is consistent with the $z \sim 0.07$ – 0.7 mass–metallicity relations and the underlying field galaxy population.

4.5. Locations: Projected Physical and Host-normalized Offsets

Last we consider the projected physical offsets (ρ) of the expanded sample of FRBs, in addition to the projected offsets normalized by the half-light radii of the hosts (ρ/R_{eff}). When

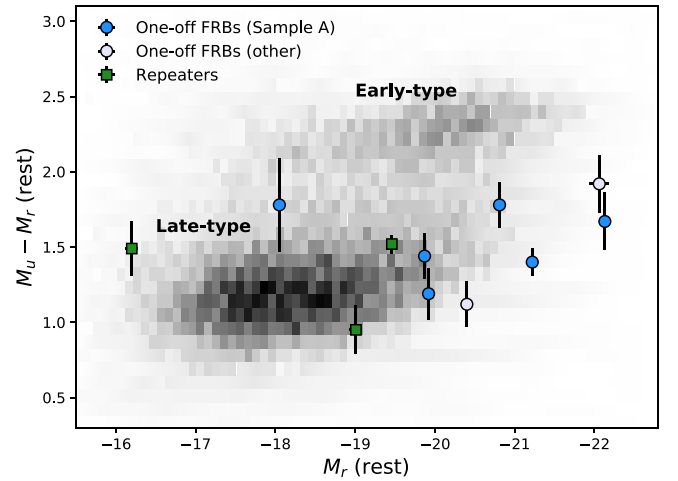


Figure 5. Rest-frame color–magnitude diagram of the host galaxies of repeating and nonrepeating FRBs compared to the underlying field galaxy population from the PRIMUS survey (Moustakas et al. 2013). The FRB symbol notations are identical to Figure 4. The majority of the FRB hosts are part of the brightest galaxy population.

Table 4

P -values Obtained via 2D KS Tests with the Null Hypothesis That an FRB-host Galaxy Population (One-off, Repeating, or All) is Drawn from the Same Underlying Distribution as Early- or Late-type Galaxy Populations or the Full Distribution

| Galaxy Type | P_{KS} (one-off) | P_{KS} (rep.) | P_{KS} (all) |
|-------------|--------------------|-----------------|----------------|
| All | 0.002 | 0.178 | 0.007 |
| Early-type | <0.001 | <0.001 | <0.001 |
| Late-type | <0.001 | 0.192 | <0.001 |

operating in the ICS mode, ASKAP/CRAFT can now deliver subarcsecond localizations of FRBs upon detection, without requiring the use of follow-up facilities on repeat bursts. Both approaches allow us to accurately determine the FRB emission sites with respect to their host-galaxy centers (“offsets”), which provide additional clues to the progenitors of FRBs. Indeed, the offset distributions of other transients have provided a key diagnostic for understanding their origins (discussed further in Section 5).

For each FRB in Sample A, we measure the angular offset between the FRB location and its host-galaxy center, taking into account positional and astrometric uncertainties for each measurement and use the redshift of the host galaxy to convert to physical offsets in kpc. We determine a broad range of projected physical offsets for the FRBs in Sample A, spanning from 0.6 kpc (FRB 121102) to ≈ 11 kpc (FRBs 190611 and 191001); they are listed in Table 3. Overall, we find that FRBs have significant offsets relative to the centers of their host galaxies, with median and mean values of 3.3 and 4.8 kpc, respectively. We caution that the observed FRB population presented here could be biased against small offsets due to an increasing effect of DM scattering or “smearing” caused by the dense ISM, thus decreasing the FRB detection probability closer to their host-galaxy centers. However, we expect this effect to be minor. Using the derived host-galaxy sizes (R_{eff}), we also measure the host-normalized offsets for Sample A. We caution that most of the R_{eff} values were derived from seeing-limited observations and are therefore subject to significant

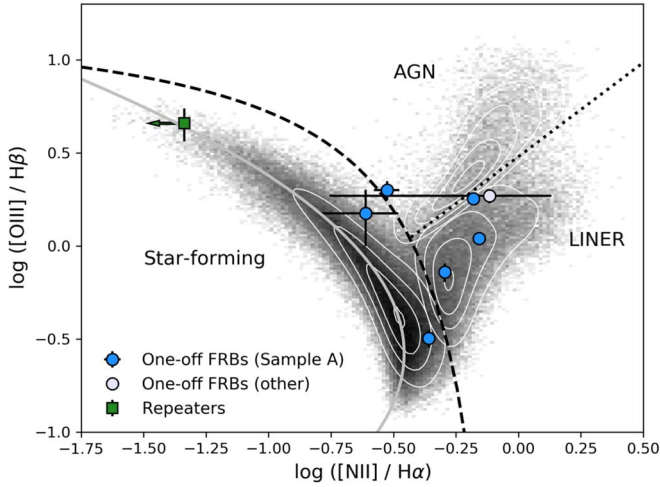


Figure 6. BPT (Baldwin et al. 1981) classification diagram for FRB hosts. The FRB symbol notations are identical to previous figures. The gray-scale background shows the density distribution of nearby ($0.02 < z < 0.4$) emission-line galaxies from the SDSS, only considering $S/N > 5$. The solid gray line follows the highest density of local SF galaxies (Brinchmann et al. 2008). The dashed and dotted black lines represent the demarcation line between SF galaxies and AGNs (Kauffmann et al. 2003) and AGN and LINERs (Cid Fernandes et al. 2010), respectively. The white contours show the KDE of the galaxy population distributions used to model their individual PDFs. The majority of FRB hosts show excess line flux ratios compared to typical SF galaxies.

Table 5

P-values Obtained via a 2D KS Test for FRB-host Populations (Considering the Full Set of Repeating and Nonrepeating Bursts and the One-off Bursts Only) and Different Galaxy Populations According to the BPT Diagram

| Galaxy Type | P_{KS} (one-off) | P_{KS} (all) |
|-------------|--------------------|----------------|
| All | 0.049 | 0.023 |
| SF | 0.004 | 0.015 |
| AGN | < 0.001 | < 0.001 |
| LINER | 0.041 | 0.012 |
| AGN-LINER | 0.122 | 0.044 |
| SF-LINER | 0.039 | 0.019 |

uncertainty for the smaller galaxies ($R_{\text{eff}} \lesssim 1''$). Nevertheless, we find a range of values, $\rho = 0.4\text{--}5.3 R_{\text{eff}}$ with median and mean values of $1.4 R_{\text{eff}}$ and $1.7 R_{\text{eff}}$, respectively. We note that this is larger than the median expected offset if FRBs traced the locations of stars in their disks (e.g., $1 R_{\text{eff}}$).

5. Implications for FRB Progenitors

We have here shown that FRB hosts exhibit very diverse environments: in particular, we observe a large variety in terms of their morphologies, ranging from early- to late-type galaxies, and found that FRB hosts are characterized by a broad, continuous range of rest-frame colors, luminosities, stellar masses, SFRs and ages. We now explore the implications for the nature of FRB progenitors through further comparisons of their host-galaxy properties to the hosts of other astronomical transients.

5.1. Comparisons to the Host Properties and Offset Distributions of Other Transients

The host galaxies of other known transients such as LGRBs, SGRBs, CC, and SNe Ia provide a natural baseline for

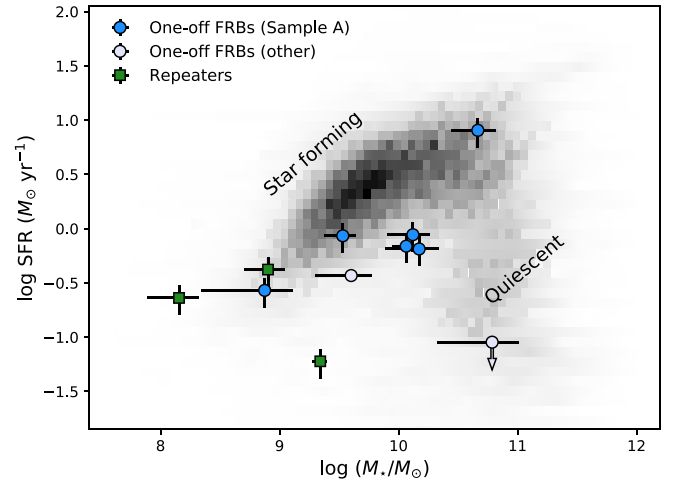


Figure 7. Star formation rate vs. stellar mass M_* distribution of FRB hosts. The error bars on the SFR estimates also take into account the scatter in the $\text{SFR} - L_{\text{H}\alpha}$ relation. The FRB symbol notations are again identical to previous figures, and we here also include the galaxies from the PRIMUS survey as the background sample. Because some of the hosts show LINER-like emission, the SFR should potentially be treated as an upper limit (see main text). The hosts of repeating FRBs show more diverse behavior: i.e., starbursts (FRB 121102), regular SF (FRB 190711), and quiescent (FRB 180916) galaxies compared to the hosts of nonrepeating FRBs.

comparison to the FRB-host population because these have been intensively studied, and have known or likely known progenitors. Investigating the connection between their hosts and galaxies hosting FRBs can therefore provide important (though indirect) clues to the most likely FRB progenitor channels. Based on the first small samples of FRB-associated hosts (Bhandari et al. 2020b; Li & Zhang 2020), it was already evident that the majority had generally high masses and low SFRs (excluding FRB 121102). Our work has further cemented this picture based on a sample of 10 secure host galaxies.

5.1.1. Luminosity, SFR, and Stellar Mass

Here, we further discuss the connection between FRB hosts and those of other astronomical transients and compare them quantitatively. The typically high luminosities and stellar masses but modest SFRs observed in this work are generally consistent with the galaxy populations hosting CC-SNe and SGRBs, which are found to predominantly occur in luminous, massive galaxies (Prieto et al. 2008; Berger 2009; Kelly & Kirshner 2012; Taggart & Perley 2019). These physical properties are in stark contrast to the typically elevated specific SFRs ($\text{sSFR} = \text{SFR}/M_*$) observed for the hosts of LGRBs. Moreover, the host galaxies of LGRBs at $z \lesssim 1$ are typically at the faint, low-mass end of the SF galaxy population (Savaglio et al. 2009; Schulze et al. 2015; Vergani et al. 2015; Perley et al. 2016), in contrast to what we have observed for the majority of FRB hosts.

In Figure 10 we compare the stellar mass distribution of the FRB hosts to the host galaxies of these other transients, namely SGRBs (Nugent et al. 2020), LGRBs (Vergani et al. 2015), and CC-SNe (Schulze et al. 2020). To mitigate the effects of the cosmological evolution of galaxies and ensure a fair comparison, we require $z < 1$ for the host galaxies for all of the comparison samples. The M_* CDF for FRBs is intermediate between the lower mass hosts of LGRBs and the higher mass hosts of SGRBs, and most closely following those of CC-SNe.

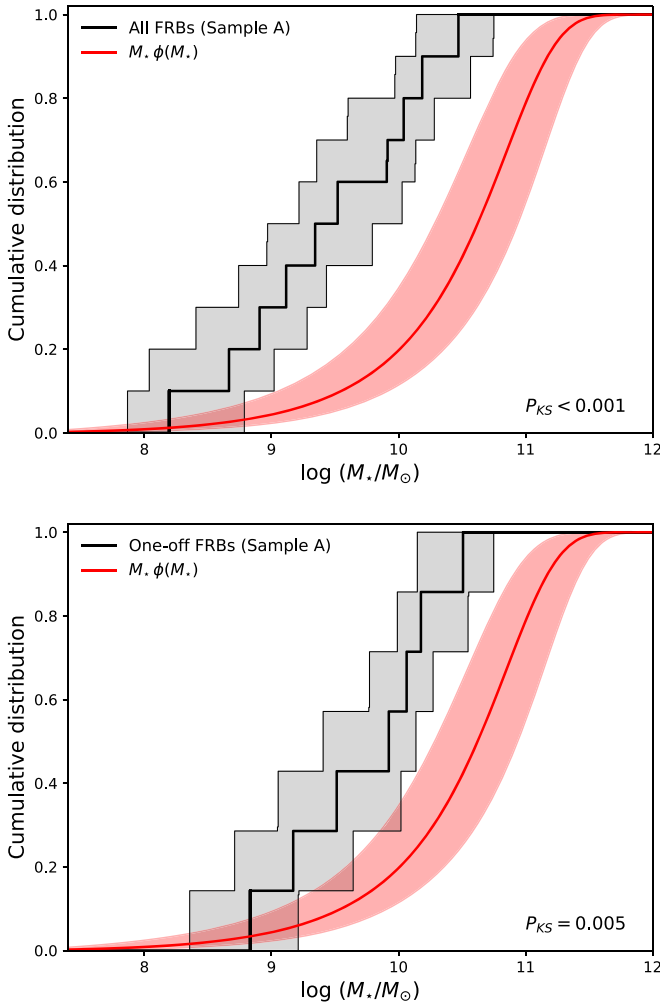


Figure 8. Stellar mass M_* cumulative distribution of all (top panel) and only the nonrepeating (bottom panel) FRB hosts in Sample A. The gray shaded region represents the 1σ uncertainty on the CDF, combining the error on the measurements and due to the sample size (see text for details). The observed distribution is compared to the stellar mass function $\phi(M_*)$ for the full COSMOS sample from Davidzon et al. (2017; at $0.2 < z < 0.5$), assuming a mass-weighted selection $M_* \phi(M_*)$ from the field galaxy mass function (red line). The computed P -values from a one-sided KS test between the distributions are listed at the bottom of both panels.

Neither of the SGRB or CC-SNe host populations, however, has statistically inconsistent CDFs. When the comparison is restricted to the one-off FRBs, the correspondence to the host galaxies of LGRBs is further disfavored with $P_{KS} < 0.05$.

5.1.2. No Evidence for Metal Aversion in FRB Hosts

As was demonstrated in Section 4.4, the stellar masses and metallicities of FRB hosts are generally consistent with the mass–metallicity relations observed for field galaxies at $z = 0.07$ – 0.7 . This is again consistent with the host galaxies of SGRBs at $z < 1$ (Berger 2009) and CC (Type II)/SNe Ia (Prieto et al. 2008), which are also found to closely track the mass–metallicity or luminosity–metallicity relations of field galaxies at similar redshifts. In contrast, the production of LGRBs appears to be heavily suppressed in more metal-rich environments (at least at $z < 1$; Perley et al. 2016) compared to

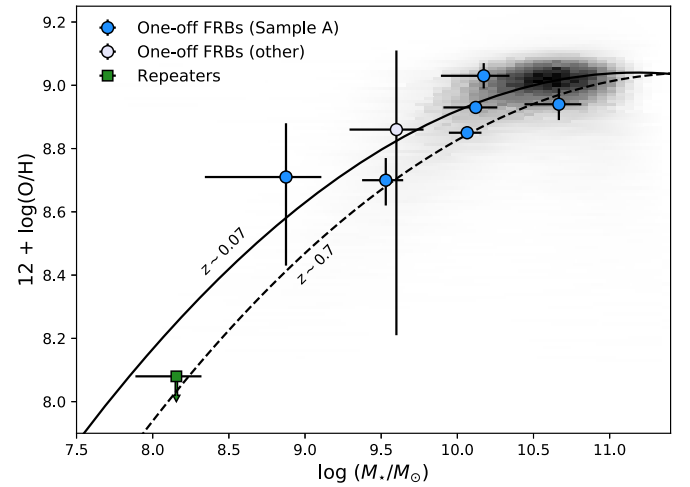


Figure 9. Mass–metallicity relation of FRB hosts. The FRB symbol notations are identical to previous figures. Here, we only show a subset of the FRB hosts for which sufficient emission-line fluxes have been measured to derive or place limits on the oxygen abundance $12 + \log(\text{O}/\text{H})$, assuming the Hirschauer et al. (2018) O3N2 calibration, see Table 2. For the gray-scale background distribution, we again use the local SDSS emission-line sample. For reference, the mass–metallicity relations from Maiolino et al. (2008) are shown for $z \sim 0.07$ (solid) and $z \sim 0.7$ (dashed).

field galaxies at similar masses. FRB progenitors show no such metallicity bias in their host galaxies.

5.1.3. Physical and Host-normalized Offsets

We then compare the physical and host-normalized offset distributions of FRBs to that of the SGRB (Fong & Berger 2013, W. Fong et al. 2020, in preparation), LGRB (Blanchard et al. 2016), and CC/SNe Ia (Prieto et al. 2008; Kelly & Kirshner 2012) populations in Figure 11. For context, the locations of LGRBs match expectations for the H II regions of massive stars in an exponential disk, commensurate with their massive star progenitors (Bloom et al. 2002; Blanchard et al. 2016; Lyman et al. 2017). For SGRBs, which originate from older stellar populations, the broad range of projected offsets of SGRBs extending to tens of kiloparsec are believed to result from neutron star kicks and delay times, providing a strong link to their neutron star merger progenitors (Fong & Berger 2013).

In comparison, it is already evident that most FRBs are not coincident with the nucleus of their hosts, disfavoring models involving AGN or supermassive black holes in general (see Figure 1; and also Bhandari et al. 2020b). The offset distribution of the full sample of FRBs is found to closely follow the observed distribution of CC and SNe Ia, with one-sided KS tests yielding $P_{KS} = 0.96$ and $P_{KS} = 0.95$, respectively. The FRB and SGRB offset distributions are also consistent, but a larger fraction of SGRBs are observed to occur at even greater distances from their host-galaxy centers (Fong & Berger 2013), which is more consistent with theoretical expectations of binary neutron star mergers (Fryer & Kalogera 1997; Bloom et al. 1999; Belczynski et al. 2006). We find similar results when we restrict our analysis to the hosts of one-off FRBs. On the other hand, LGRBs are observed to be one of the most centrally concentrated populations, which is inconsistent with that of FRBs (with $P_{KS} = 0.008$).

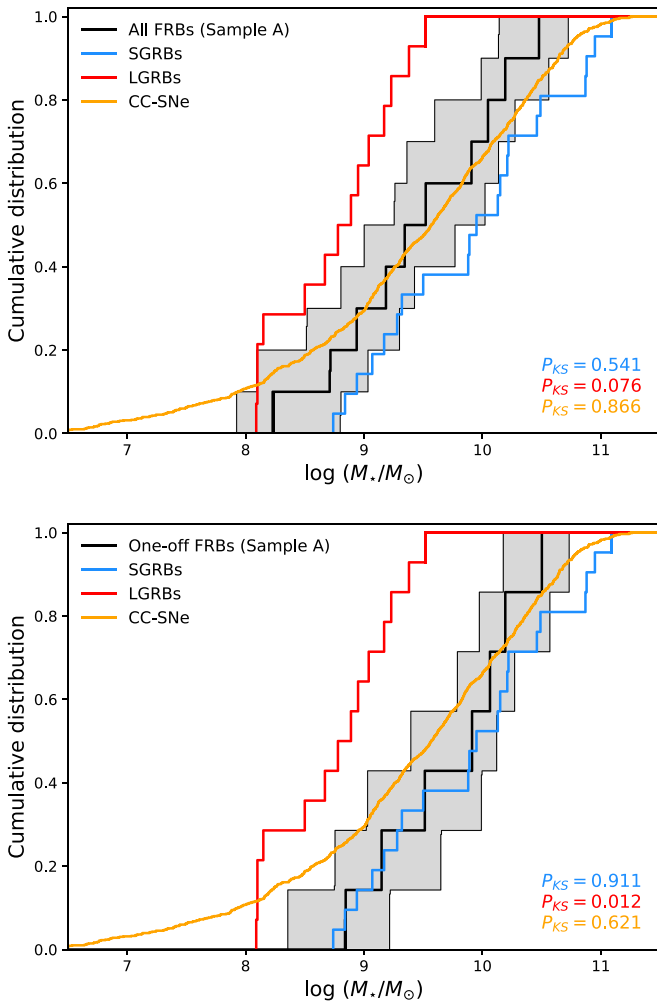


Figure 10. Stellar mass M_* cumulative distribution of all (top panel) and only the nonrepeating (bottom panel) FRB hosts in Sample A. The gray shaded region represents the 1σ uncertainty on the CDF, combining the error on the measurements and that due to the sample size (see Section 4.3 for details). For comparison, we overplot samples of SGRB (blue; Nugent et al. 2020), LGRB (red; Vergani et al. 2015), and CC-SN (orange; Schulze et al. 2020) hosts, all at $z < 1$. The computed P -values from a two-sided KS test are listed for the comparison distribution functions relative to the FRB samples.

When the offsets are normalized by the effective radii of the host galaxies (Figure 11, right), the results are qualitatively similar, although the LGRB distribution is no longer inconsistent at high confidence.

5.1.4. Implications for FRB Progenitor Channels

Because the progenitors of FRBs (and astronomical transients in general) are linked to specific stellar populations and galaxy environments, determining these host-galaxy properties also allows us to place constraints on the likely progenitor channels of FRBs. Based on the similar properties of the first identified FRB host (that of the repeater, FRB 121102) to those of LGRBs and SLSNe (Tendulkar et al. 2017), a possible common progenitor channel of “young” magnetar remnants producing FRBs was proposed (Metzger et al. 2017; Nicholl et al. 2017). FRB 121102 originated from a low-mass and intensely SF galaxy relative to the typical FRB-host-galaxy population (Li et al. 2019; Bhandari et al. 2020b). With the addition of two repeaters, FRBs 180916 and 190711, as well as

the expanded sample of the hosts of apparent one-off FRBs studied here, the host properties exhibit a more continuous function in terms of their luminosities, stellar masses, and SFRs than previous studies. In the context of the sample of 13 hosts studied here, we note that FRB 121102 is still on the extreme end in terms of its host properties (e.g., metal-deficient, low stellar mass, high SFR, and low luminosity).

Finally, a metal deficit and high SFR per unit stellar mass seem to be crucial for the probability of a nearby ($z < 1$) galaxy to host LGRBs or SLSNe. No such restrictions appear to govern the production of FRBs. We can thus conclude that the rapidly rotating massive stars that are believed to produce LGRBs (Woosley & Heger 2006) are unlikely to constitute the majority of progenitors producing FRBs (Marnoch et al. 2020). This conclusion is supported by the presence of some FRBs in galaxies with older stellar populations.

Instead, out of the other progenitor models proposed thus far, the physical properties of the FRB hosts are most similar to the host populations of SGRBs and CC/SNe Ia (Bhandari et al. 2020b; Li & Zhang 2020), although with a larger fraction of quiescent, older galaxies than the CC-SNe host population. Indeed, FRBs have been proposed to originate from either young or long-lived stable magnetars produced by a variety of channels, including binary neutron star mergers (at least some of which produce SGRBs) or in the accretion-induced collapse (AIC) of white dwarfs (Moriya 2016; Margalit et al. 2019). The FRB-host properties presented here, which span the full range of properties occupied by field galaxies at similar redshifts, are currently consistent with a single progenitor that can accommodate a diverse set of host properties, although contributions from multiple progenitors cannot be ruled out. Coupled with the similarities found when compared to both SGRB and SNe Ia host properties, magnetars produced as a result of binary neutron star mergers and/or white dwarf scenarios (e.g., Kashiyama et al. 2013; Moriya 2016) remain viable FRB progenitor channels. In conclusion, it is clear that there is not a single preferred type of host galaxy (as is the case for LGRBs or SLSNe), and that any progenitor model will have to confront the diverse set of galaxy properties exhibited by the FRB-host population, as well as the relationships to the underlying galaxy population.

5.2. Is the Milky Way a Typical FRB Host?

An intriguing new clue to the origin of FRBs came from the discovery of a brief radio burst from the Galactic magnetar/soft gamma repeater SGR 1935+2154 (Bochenek et al. 2020a; Scholz & Chime/Frb Collaboration 2020). The released radio energy in this event is approximately two orders of magnitude lower than that observed for the weakest of the cosmological FRBs (Bochenek et al. 2020b; The CHIME/FRB Collaboration et al. 2020), and approximately five orders of magnitude fainter than typical one-off bursts (such as FRBs 180924 and 181112). This is not unexpected, however, because such weak bursts would be difficult to detect at $z \gtrsim 0.1$, and this Galactic “FRB” might therefore represent the faint end of the observed extragalactic FRB distribution.

To further examine this possibility, we can now pose the question whether the Milky Way is a typical FRB-host galaxy. Based on the inferred properties of $M_{*,MW} = (6.08 \pm 1.14) \times 10^{10} M_\odot$ and $SFR_{MW} = 1.65 \pm 0.19 M_\odot \text{ yr}^{-1}$ (Licquia & Newman 2015), we find that the Milky Way is indeed consistent with being a typical FRB-host galaxy. Its $SFR-M_*$

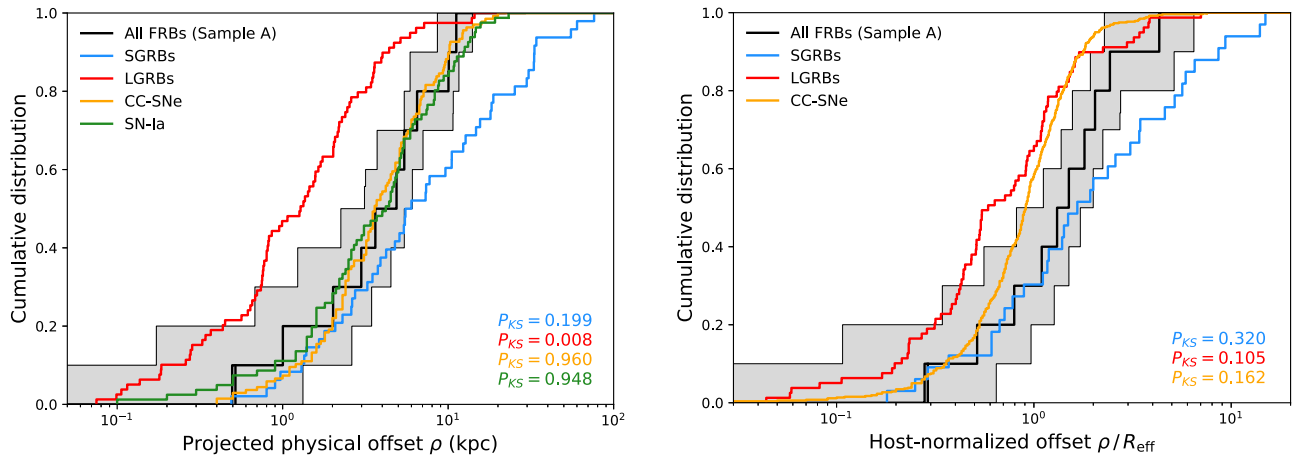


Figure 11. Cumulative distribution of projected physical offsets ρ (left) and host-normalized offsets ρ/R_{eff} (right) for all FRBs (in Sample A). The gray shaded region again represents 1σ uncertainty on the CDF, combining the error on the measurements and that due to the sample size. Reference samples of SGRBs (blue; Fong et al. 2010; Fong & Berger 2013; W. Fong et al. 2020, in preparation), LGRBs (red; Blanchard et al. 2016), CC-SNe (orange; Prieto et al. 2008; Kelly & Kirshner 2012), and SNe Ia (green; Prieto et al. 2008) are shown for comparison. The effective radii of the SNe Ia were not available to determine their host-normalized offset distribution. The computed P -values from a two-sided KS test are again listed for the comparison distribution functions relative to the total FRB sample. The FRB projected physical offset distribution is intermediate between the LGRB and SGRB distributions, but closely follows the CC and SN Ia offset distributions. When only the host-normalized offsets are considered, the distributions between the different types of transients becomes less distinct.

relation places it in the transition region between SF and quiescent galaxies, intermediate to what has been observed for the most massive ($M_* > 10^{10} M_\odot$) FRB hosts. The same is true for the mass–metallicity relation of the Milky Way. Our Galaxy is thus a typical FRB-host galaxy. In addition, SGR 1935+2154 is located approximately 9 kpc from the Galactic center (Kotthes et al. 2018; Bochenek et al. 2020b), which is in the high end of the physical offset distribution of the burst sites observed here. All these considerations further support the connection between the radio emission from SGR 1935+2154 and low-luminosity FRBs.

6. Summary and Outlook

Here, we have presented new observations of five host galaxies of arcsecond-localized FRBs, together with a comprehensive analysis of their stellar population properties (colors, metallicities, luminosities, stellar masses, mass-weighted ages, and SFRs) and locations with respect to their host-galaxy centers. One of these FRBs (FRB 190711) is confirmed to be a repeating event, whereas the remaining four are apparently nonrepeating.

We explored these properties in the context of all previously reported hosts of well-localized events: 10 FRB-host galaxies detected by CRAFT/ASKAP, as well as 3 additional FRBs discovered by other surveys (CHIME, DSA, and Arecibo). The precise localizations of these events enabled us to determine the most likely host-galaxy associations and define a “gold” sample (Sample A) of 10 hosts on which we based our statistical analyses. Of these hosts, 3 are known repeaters and 7 are (apparently) one-off bursts. To homogenize the results and present a uniform analysis that is not subject to systematic differences in stellar population modeling across several works, we obtained additional spectroscopic and photometric data of all 10 FRB hosts in Sample A and presented new SED modeling and spectral fits based on these observations (including the 4 host galaxies presented in Bhandari et al. 2020b). This work represents the largest sample of FRB-host galaxies to date and enables a statistical examination relative to

the field galaxy population and to hosts of other transient types, as well as an exploration between known repeaters and (apparently) one-off bursts. The main results were as follows.

1. The majority of FRB hosts populate the range between $L \sim 0.1L^* - L^*$ at $z < 0.7$. We find a tendency for the hosts of known repeating FRBs to exhibit colors of late-type galaxies, and to be overall less luminous and have lower stellar masses than the average FRB host.
2. The full sample spans a large, continuous range in color ($M_u - M_r = 0.9\text{--}2.0$), mass-weighted stellar population age (0.06–1.6 Gyr), stellar mass ($M_* = 10^8 - 6 \times 10^{10} M_\odot$), and SFR ($\text{SFR} = 0.05\text{--}10 M_\odot \text{ yr}^{-1}$) spanning the full parameter space occupied by $z < 0.5$ galaxies. While the hosts of nonrepeating FRBs are typically more massive than the average population of galaxies on the SF main sequence, the hosts of repeating FRBs exhibit much more diversity, ranging from starburst (FRB 121102), to regular SF (FRB 190711), to more quiescent (FRB 180916) galaxies.
3. Statistical tests revealed that the mass distributions of the FRB hosts can be ruled out ($>99.9\%$ c.l.) as being uniformly drawn from the underlying mass distribution of field galaxies at a similar redshift range. This implies that FRBs do not directly track stellar mass.
4. The majority of FRB hosts are emission-line galaxies, but with line ratios in the BPT diagram that do not track the distribution of regular field galaxies. In particular, the FRBs exhibit a high incidence of cases in the LINER population, which is indicative of a harder radiation field.
5. The overall sample of FRB hosts were found to be metal rich, with oxygen abundances distributed between $12 + \log(\text{O}/\text{H}) = 8.7\text{--}9.0$ (the exception being the host of FRB 121102 with $12 + \log(\text{O}/\text{H}) < 8.08$), although all are consistent with the $z \sim 0.07\text{--}0.7$ mass–metallicity relations and the underlying field galaxy population.
6. The physical offsets from the FRB position to the host-galaxy centers range from 0.6 to 11 kpc, with a median value of 3.3 kpc. Normalizing these by the half-light radii

R_{eff} of the host galaxies yields host-normalized offsets ranging from 0.4 to 5.3 R_{eff} with a median of 1.4 R_{eff} .

7. Comparing the host-galaxy properties and the projected physical offsets of FRBs to those observed for the populations of other transients (SGRBs, LGRBs, and CC, and SNe Ia) allowed us to place empirical constraints on potential stellar transients accompanying (or preceding) the FRB events. We found that the generally massive and metal-rich environments of the FRB hosts disfavor similar progenitor channels to those producing LGRBs (with FRB 121102 being the exception). Moreover, the FRB host-burst offset distribution is consistent with those observed for SGRBs, CC, and SNe Ia, and further disfavors LGRBs ($>99\%$ c.l.).
8. Based on the host properties alone, magnetars formed via binary neutron star mergers, accretion-induced collapses of white dwarfs, or regular CC-SNe are thus among the current most plausible mechanisms for the majority of the FRB population. Any progenitor models also have to accommodate the broad, continuous range of host-galaxy properties, likely reflecting a large variety in type or lifetime of FRB progenitors.

This work highlights the crucial role of \sim arcsecond-level localizations in making robust associations with host galaxies (e.g., Eftekhari & Berger 2017) and delineating the progenitors of FRBs. The associations are made even more challenging by the fact that the FRBs localized thus far exhibit substantial offsets from their host galaxies. It is particularly notable that one-off FRBs do not appear to be drawn from more typical galaxies. If so, a prior may be to search less ordinary galaxies to determine the hosts of FRBs that are poorly localized. In the future, larger samples of FRB-host galaxies will further establish whether the typical physical properties discovered here are common for the full population of FRBs. In particular, a larger number of galaxies hosting known repeating FRBs needs to be observed to decisively conclude the relationship between known repeating and apparently nonrepeating FRBs, as gleaned from their host-galaxy environments. Because FRBs are observed to originate in a diversity of galaxies, it is also crucial to study the local environments of their burst sites. Understanding the FRBs and their environments better will also significantly aid in their use as cosmological probes.

We would like to thank the referee for a thorough and constructive report, greatly improving the presentation of the results from this work. We would also like to thank Johan P. U. Fynbo and Enrico Ramirez-Ruiz for enlightening discussions on the implications for FRB progenitor models and Jesse Palmerio for his insight into statistical modeling. We would also like to thank Vikram Ravi for sharing his images of the host galaxy and localization region of FRB 190523. K.E.H. acknowledges support by a Project Grant (162948–051) from The Icelandic Research Fund. The Fast and Fortunate for FRB Follow-up team acknowledges support from NSF grants AST-1911140 and AST-1910471. N.T. acknowledges support by FONDECYT grant 11191217. W.F. acknowledges support by the National Science Foundation under grant No. AST-1814782. K.A. acknowledges support from NSF grant AAG-1714897. A.T.D. is the recipient of an ARC Future Fellowship (FT150100415). R.M.S. acknowledges support through ARC Future Fellowship FT190100155 and discovery project DP180100857. This work is partly based on observations

collected at the European Southern Observatory under ESO programs 0103.A-0101(A) and 0103.A-0101(B). This work is partly based on observations obtained at the international Gemini Observatory, a program of NSF's OIR Lab, which is managed by the Association of Universities for Research in Astronomy (AURA) under a cooperative agreement with the National Science Foundation, on behalf of the Gemini Observatory partnership: the National Science Foundation (United States), National Research Council (Canada), Agencia Nacional de Investigación y Desarrollo (Chile), Ministerio de Ciencia, Tecnología e Innovación (Argentina), Ministério da Ciência, Tecnologia, Inovações e Comunicações (Brazil), and Korea Astronomy and Space Science Institute (Republic of Korea). The Gemini data were obtained from program GS-2019B-Q-132, and processed using the Gemini PYRAF package.²³ The Australian Square Kilometre Array Pathfinder and Australia Telescope Compact Array are part of the Australia Telescope National Facility, which is managed by CSIRO. Operation of ASKAP is funded by the Australian Government with support from the National Collaborative Research Infrastructure Strategy. ASKAP uses the resources of the Pawsey Supercomputing Centre. Establishment of ASKAP, the Murchison Radio-astronomy Observatory, and the Pawsey Supercomputing Centre are initiatives of the Australian Government, with support from the Government of Western Australia and the Science and Industry Endowment Fund. We acknowledge the Wajarri Yamatji as the traditional owners of the Murchison Radio-astronomy Observatory site. Partly based on observations made with the Nordic Optical Telescope, operated by the Nordic Optical Telescope Scientific Association at the Observatorio del Roque de los Muchachos, La Palma, Spain, of the Instituto de Astrofísica de Canarias. Some of the data presented herein were obtained at the W. M. Keck Observatory, which is operated as a scientific partnership of the California Institute of Technology, the University of California and the National Aeronautics and Space Administration. The Observatory was made possible by the generous financial support of the W. M. Keck Foundation. The authors wish to recognize and acknowledge the very significant cultural role and reverence that the summit of Maunakea has always had within the indigenous Hawaiian community. We are most fortunate to have the opportunity to conduct observations from this mountain. W. M. Keck Observatory access for FRB200430 was supported by Northwestern University and the Center for Interdisciplinary Exploration and Research in Astrophysics (CIERA).

Appendix A

Updated Literature FRB Host Properties

A.1. ASKAP/CRAFT

FRB 180924, FRB 181112, FRB 190102, FRB 190608, and FRB 191001. All of these FRBs and their host galaxies were presented in previous CRAFT publications (Bannister et al. 2019; Prochaska et al. 2019a; Bhandari et al. 2020a, 2020b; Chittidi et al. 2020; Macquart et al. 2020). Several of the FRB coordinates have been improved from refined analysis of the saved baseband data, enabling more precise positions for the FRBs and/or a better estimate of the astrometric registration of the FRB image (Day et al. 2020). For FRB 190102 we also

²³ <https://www.gemini.edu/sciops/data-and-results/processing-software>

include the HST/F160W band photometry measured by A. Mannings et al. (2020, in preparation) of $m_{F160W} = 20.45 \pm 0.01$ mag in the SED fit of the host galaxy to improve the estimates of the stellar population parameters. We note that for FRB191001, the R.A. uncertainty reported in Bhandari et al. (2020a) of 0.006s was incorrectly calculated, and should have been 0.02s (the latter adopted in this work). All of these except for FRB 181112 are included in Sample A. While we still maintain the association of FRB 181112 to DES J214923.66–525815.28 to be highly secure, the foreground galaxy studied in Prochaska et al. (2019a) is sufficiently bright to also give $P_{\text{chance}} < 0.05$. Therefore this association places it within Sample C. A future Bayesian framework for FRB-host associations will enable a direct comparison of the probabilities of the two sources, and we expect that DES J214923.66–525815.28 will be highly favored.

FRB 190714 and FRB 200430. The final positions and uncertainties for these FRBs were determined following the method used for all previous ASKAP/CRAFT FRBs (for detailed descriptions of this method, see Bannister et al. 2019; Prochaska et al. 2019a; Day et al. 2020; Macquart et al. 2020). Briefly, the statistical position and uncertainty in R.A. and decl. are derived by fitting a 2D Gaussian to a region containing the FRB in a Stokes *I* frequency-averaged image. Any errors in the phase-calibration solutions (due to the spatial and temporal differences in the FRB and calibrator observations) are corrected for by comparing the positions of continuum field sources detected in an image made with the 3.1 s of voltage data containing the FRB to positions from reference catalogs, thereby aligning the ASKAP reference frame with the International Celestial Reference Frame (ICRF3). The systematic uncertainties and any offsets are then determined following the method described in Macquart et al. (2020). The statistical FRB position is then corrected for any offset, with the final uncertainty being the quadrature sum of the statistical and systematic uncertainties.

For FRB 190714, two quick-look images from the Karl G. Jansky Very Large Array Sky Survey (VLASS, Lacy et al. 2020) were used for comparison with the ASKAP field sources, with offsets and systematic uncertainties in R.A. and decl. determined to be $0''.71 \pm 0''.32$ and $-1''.45 \pm 0''.23$, respectively. For comparison with the FRB 200430 field sources, catalog positions from the Faint Images of the Radio Sky at Twenty centimetres (FIRST, Becker et al. 1995) survey were used and offsets and uncertainties determined as above. Unusually, FRB 200340 exhibits a dependence of position in decl. on frequency (yielding an offset in decl. $\approx 7''$ across the frequency band). This indicates a frequency-dependent phase error, potentially due to the ionosphere. Because the FRB and field sources have different spectral indices, their frequency-averaged centroids will likewise differ. In order to account for the bias introduced in correcting the FRB position with the field sources, a coarse spectral index of the FRB was determined by performing a linear fit to the log of the flux densities (extracted from a 56 MHz resolution image cube of the FRB) versus frequency, yielding spectral index $\alpha = -5.46$, and compared to a typical spectral index of the field sources ($\alpha = -0.7$). This was then used to derive the expected deviation in decl. given the offset in the flux-weighted centroid frequencies (49 MHz) by evaluating a weighted linear fit of the decl. offsets in the FRB image cube versus frequency at both central frequencies. An offset of $0''.93$ was derived, which we also conservatively

take to be the typical uncertainty expected due to this bias. Combining this with the offsets and systematic uncertainties derived via the standard field-source comparison method, we obtain a total systematic offset and uncertainty in R.A. and decl. of $-0''.03 \pm 0''.25$ and $4''.12 \pm 1''.04$, respectively.

CIGALE. As noted in Section 3, we have reanalyzed the SED models of all the previously published hosts from ASKAP/CRAFT using the same set of model inputs applied to the new hosts. Because of the sensitivity of M_* and SFR to assumptions on the SFH and dust, the new values are quantitatively different. This is reflected by their large uncertainties, but we caution that the results are further subject to systematic errors related to model assumptions. In one case (FRB 190608), we also identified an error in our database that led to the misreporting of results in Bhandari et al. (2020b).

A.2. CHIME

FRB 180916. Marcote et al. (2020) reported the first FRB discovered by the CHIME experiment (CHIME/FRB Collaboration et al. 2018) to be localized to high-precision, FRB 180916.J0158+65 (hereafter FRB 180916 for convenience). It is coincident with the spiral arm of the previously cataloged galaxy SDSS J015800.28+654253.0. As detailed by these authors, the probability of a chance association is very low, and our own estimate is $P_{\text{chance}} = 0.0059$. We therefore include it in Sample A.

We also performed SED modeling of the host with CIGALE, using archival SDSS optical and mid-infrared WISE photometric data. We compute a stellar mass of $M_* = (2.15 \pm 0.33) \times 10^9 M_\odot$, which is approximately a factor of five lower than the estimate by Marcote et al. (2020). We caution that both of these estimates suffer from large systematic uncertainties due to the substantial corrections for Galactic extinction.

A.3. DSA

FRB 190523. Ravi et al. (2019) reported the detection of FRB 190523 with the Owens Valley DSA observatory. The $3'' \times 8''$ 95% error ellipses is nearly coincident with the centers of two sources labeled S1 and S2 by these authors (at J134815.44+722814.72 and J134815.74+722805.9, respectively). Ravi et al. (2019) favor associating S1 with the FRB owing to its somewhat closer angular offset ($\theta_{S1} = 3''.8$ versus $\theta_{S2} \approx 5''.1$) and because its spectroscopic redshift $z_{\text{spec}} = 0.660$ agrees well with the Macquart DM– z relation (Macquart et al. 2020). Based on the formalism for associations adopted here (Section 2.1), we find $P_{\text{chance}}(\text{S1}) = 0.07$ and $P_{\text{chance}}(\text{S2}) = 0.10$.

Subsequent to the Ravi et al. (2019) publication, we observed S1 and S2 with the DEIMOS spectrograph on the Keck II telescope (Prochaska et al. 2019b). The instrument was configured with the 600ZD grating tilted to cover $\lambda \approx 5000$ – 9500 Å and the $1''$ longslit yields a resolution $R \approx 2500$. These data were reduced using the PyPeIt software package in the same manner as described above. These data confirm the redshift of S1 reported by Ravi et al. (2019) and yield a spectroscopic redshift for S2 of $z_{\text{spec}} = 0.363$ based on H α and [N II] nebular emission.

We here revisit the effective prior adopted by Ravi et al. (2019) by adopting the DM– z relation. These authors report $\text{DM}_{\text{FRB}} = 760.8 \text{ pc cm}^{-3}$, and the Galactic ISM contribution along this sightline is $\text{DM}_{\text{MW,ISM}} = 37 \text{ pc cm}^{-3}$. Assuming a Galactic halo contribution of $\text{DM}_{\text{MW,halo}} = 50 \text{ pc cm}^{-3}$

(Prochaska & Zheng 2019; Platts et al. 2020, but see Keating & Pen 2020) and a host contribution of 80 pc cm^{-3} in the host rest-frame, we have an estimated cosmic dispersion measure of $\text{DM}_{\text{cosmic}}(\text{S1}) = 625 \text{ pc cm}^{-3}$ and $\text{DM}_{\text{cosmic}}(\text{S2}) = 616 \text{ pc cm}^{-3}$ for each source. These are to be compared against the average cosmic dispersion measure to the redshift of each galaxy, $\langle \text{DM}_{\text{cosmic}} \rangle(\text{S1}) = 607 \text{ pc cm}^{-3}$ and $\langle \text{DM}_{\text{cosmic}} \rangle(\text{S2}) = 319 \text{ pc cm}^{-3}$ for each source. Even allowing for many tens of pc cm^{-3} uncertainty in the $\text{DM}_{\text{MW,halo}}$ and DM_{host} terms that contribute to the $\text{DM}_{\text{cosmic}}$ estimate, the observations favor S1. In any event, neither candidate satisfies $P_{\text{chance}} < 0.05$, and we place this association in Sample C and associate S1 with the FRB.

A.4. *Realfast*

FRB 190614. Law et al. (2020) report the first putative detection of an FRB from the *realfast* collaboration (Law et al. 2018), FRB 20190614D (here referred to as FRB 190614). They further report the galaxy pair J042017.71+734222.9 and J042017.87+734224.4 at separations $\approx 1''.5$ from the FRB centroid and estimate chance probabilities for both galaxies of $P_{\text{chance}}(\text{A}, \text{B}) = 0.07$. Despite follow-up spectroscopy with the Keck I telescope, neither has a secure spectroscopic redshift.

Photometric analysis yields $z_{\text{phot}} = 0.6$ for each galaxy with uncertainties of 0.15, 0.2 for A and B respectively. These are roughly consistent with the large dispersion measure reported for FRB 190614. In our analysis, we have adopted J042017.87+734224.4 as the host, but we include this system in Sample D.

A.5. *Others*

FRB 121102. The host galaxy of FRB 121102 (also known as “the Repeater”) was studied in detail by Tendulkar et al. (2017). We adopt the majority of their measurements here, but use the updated coordinates for the host galaxy centroid in addition to the estimate of the galaxy’s effective half-light radius R_{eff} from Bassa et al. (2017). The probability of a chance coincidence with the host is $P_{\text{chance}} = 0.002$, and we include this system in Sample A.

Appendix B Photometric Data

The photometric data for the full set of FRB hosts considered in this work are provided in Tables 6–8.

Table 6
Photometry

| Filter | HG121102 | HG180916 | HG180924 | HG181112 | HG190102 | HG190523 | HG190608 | HG190611 | HG190711 | HG190714 | HG191001 | HG200430 |
|-------------|----------|----------|----------|----------|----------|----------|----------|----------|----------|----------|----------|----------|
| DES | | | | | | | | | | | | |
| g | | | 21.56 | 22.64 | | | | | | | 19.12 | |
| $\sigma(g)$ | | | 0.03 | 0.09 | | | | | | | 0.00 | |
| r | | | 20.50 | 21.68 | | | | | | | 18.34 | |
| $\sigma(r)$ | | | 0.02 | 0.05 | | | | | | | 0.00 | |
| i | | | 20.11 | 21.46 | | | | | | | 17.91 | |
| $\sigma(i)$ | | | 0.02 | 0.06 | | | | | | | 0.00 | |
| z | | | 19.83 | 21.42 | | | | | | | 17.74 | |
| $\sigma(z)$ | | | 0.02 | 0.11 | | | | | | | 0.00 | |
| Y | | | 19.79 | 21.05 | | | | | | | 17.63 | |
| $\sigma(Y)$ | | | 0.06 | 0.17 | | | | | | | 0.01 | |
| Pan-STARRS | | | | | | | | | | | | |
| g | | | | | | 22.92 | | | | 21.20 | | 22.16 |
| $\sigma(g)$ | | | | | | 0.17 | | | | 0.04 | | 0.08 |
| r | | | | | | 22.01 | | | | 20.69 | | 21.51 |
| $\sigma(r)$ | | | | | | 0.10 | | | | 0.03 | | 0.06 |
| i | | | | | | 21.14 | | | | 20.38 | | 21.16 |
| $\sigma(i)$ | | | | | | 0.06 | | | | 0.02 | | 0.04 |
| z | | | | | | 20.79 | | | | 20.05 | | 20.91 |
| $\sigma(z)$ | | | | | | 0.06 | | | | 0.03 | | 0.07 |
| y | | | | | | 20.59 | | | | 20.04 | | 20.67 |
| $\sigma(y)$ | | | | | | 0.10 | | | | 0.05 | | 0.18 |
| SDSS | | | | | | | | | | | | |
| u | | 20.31 | | | | | 18.99 | | | | | |
| $\sigma(u)$ | | 1.78 | | | | | 0.09 | | | | | |
| g | | 17.08 | | | | | 18.02 | | | | | |
| $\sigma(g)$ | | 0.08 | | | | | 0.02 | | | | | |
| r | | 16.17 | | | | | 17.55 | | | | | |
| $\sigma(r)$ | | 0.03 | | | | | 0.01 | | | | | |
| i | | 15.93 | | | | | 17.22 | | | | | |
| $\sigma(i)$ | | 0.02 | | | | | 0.02 | | | | | |
| z | | 15.85 | | | | | 17.09 | | | | | |
| $\sigma(z)$ | | 0.06 | | | | | 0.05 | | | | | |

Note. All photometry has been corrected for Galactic extinction.

Table 7
Photometry

| Filter | HG121102 | HG180916 | HG180924 | HG181112 | HG190102 | HG190523 | HG190608 | HG190611 | HG190711 | HG190714 | HG191001 | HG200430 |
|-----------------------|----------|----------|----------|----------|----------|----------|----------|----------|----------|----------|----------|----------|
| WISE | | | | | | | | | | | | |
| W1 | | 14.37 | 16.84 | | | | 14.37 | | | | | |
| σ (W1) | | 0.03 | 0.10 | | | | 0.03 | | | | | |
| W2 | | 14.41 | 16.06 | | | | 13.83 | | | | | |
| σ (W2) | | 0.05 | 0.18 | | | | 0.04 | | | | | |
| W3 | | 10.56 | 11.69 | | | | 10.76 | | | | | |
| σ (W3) | | 0.08 | −999.00 | | | | 0.12 | | | | | |
| W4 | | 9.08 | 8.50 | | | | 8.65 | | | | | |
| σ (W4) | | 0.52 | −999.00 | | | | 0.41 | | | | | |
| GMOS_N | | | | | | | | | | | | |
| <i>g</i> | 23.33 | | | | | | | | | | | |
| σ (<i>g</i>) | 0.12 | | | | | | | | | | | |
| <i>r</i> | 23.73 | | | | | | | | | | | |
| σ (<i>r</i>) | 0.14 | | | | | | | | | | | |
| <i>i</i> | 23.54 | | | | | | | | | | | |
| σ (<i>i</i>) | 0.09 | | | | | | | | | | | |
| <i>z</i> | 23.49 | | | | | | | | | | | |
| σ (<i>z</i>) | 0.13 | | | | | | | | | | | |
| GMOS_S | | | | | | | | | | | | |
| <i>g</i> | | | | | | | | | 23.47 | | | |
| σ (<i>g</i>) | | | | | | | | | 0.20 | | | |
| <i>r</i> | | | | | | | | 22.07 | 23.49 | | | |
| σ (<i>r</i>) | | | | | | | | 0.15 | 0.15 | | | |
| <i>i</i> | | | | | | | | 22.34 | 22.95 | | | |
| σ (<i>i</i>) | | | | | | | | 0.15 | 0.15 | | | |
| VLT | | | | | | | | | | | | |
| <i>u</i> | | | | | 22.77 | | | | | | | |
| σ (<i>u</i>) | | | | | 0.20 | | | | | | | |
| <i>g</i> | | | 21.32 | 22.50 | 21.87 | | | | 20.47 | | 18.89 | |
| σ (<i>g</i>) | | | 0.04 | 0.04 | 0.10 | | | | 0.10 | | 0.10 | |
| <i>I</i> | | | 20.07 | 21.48 | 20.77 | | | | 19.50 | | 17.84 | |
| σ (<i>I</i>) | | | 0.02 | 0.04 | 0.05 | | | | 0.10 | | 0.10 | |
| <i>z</i> | | | | | 20.54 | | | | | | | |
| σ (<i>z</i>) | | | | | 0.20 | | | | | | | |


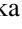











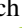

Note. All photometry has been corrected for Galactic extinction.

Table 8
Photometry

| Filter | HG121102 | HG180916 | HG180924 | HG181112 | HG190102 | HG190523 | HG190608 | HG190611 | HG190711 | HG190714 | HG191001 | HG200430 |
|-----------------------------------|----------|----------|----------|----------|----------|----------|----------|----------|----------|----------|----------|----------|
| Spitzer | | | | | | | | | | | | |
| 3.6 | 23.79 | | | | | | | | | | | |
| σ (3.6) | 0.20 | | | | | | | | | | | |
| 4.5 | 24.72 | | | | | | | | | | | |
| σ (4.5) | 999.00 | | | | | | | | | | | |
| VISTA | | | | | | | | | | | | |
| <i>Y</i> | | | | | | | | | | 18.01 | | |
| σ (<i>Y</i>) | | | | | | | | | | 0.12 | | |
| <i>J</i> | | | | | | | | | | 17.56 | | |
| σ (<i>J</i>) | | | | | | | | | | 0.09 | | |
| <i>H</i> | | | | | | | | | | 17.06 | | |
| σ (<i>H</i>) | | | | | | | | | | 0.10 | | |
| <i>K_s</i> | | | | | | | | | | 16.47 | | |
| σ (<i>K_s</i>) | | | | | | | | | | 0.20 | | |
| WFC3 | | | | | | | | | | | | |
| F110W | 23.08 | | | | | | | | | | | |
| σ (F110W) | 0.01 | | | | | | | | | | | |
| F160W | 22.96 | | | | 20.45 | | | | 22.73 | 18.88 | | |
| σ (F160W) | 0.03 | | | | 0.01 | | | | 0.01 | 0.00 | | |

Note. All photometry has been corrected for Galactic extinction.

ORCID iDs

Kasper E. Heintz  <https://orcid.org/0000-0002-9389-7413>
 J. Xavier Prochaska  <https://orcid.org/0000-0002-7738-6875>
 Sunil Simha  <https://orcid.org/0000-0003-3801-1496>
 Emma Platts  <https://orcid.org/0000-0002-9931-5672>
 Wen-fai Fong  <https://orcid.org/0000-0002-7374-935X>
 Nicolas Tejos  <https://orcid.org/0000-0002-1883-4252>
 Stuart D. Ryder  <https://orcid.org/0000-0003-4501-8100>
 Kshitij Aggerwal  <https://orcid.org/0000-0002-2059-0525>
 Shivani Bhandari  <https://orcid.org/0000-0003-3460-506X>
 Cherie K. Day  <https://orcid.org/0000-0002-8101-3027>
 Adam T. Deller  <https://orcid.org/0000-0001-9434-3837>
 Charles D. Kilpatrick  <https://orcid.org/0000-0002-5740-7747>
 Casey J. Law  <https://orcid.org/0000-0002-4119-9963>
 Lachlan J. Marnoch  <https://orcid.org/0000-0003-1483-0147>
 Ryan M. Shannon  <https://orcid.org/0000-0002-7285-6348>

References

- Abbott, T. M. C., Abdalla, F. B., Allam, S., et al. 2018, *ApJS*, **239**, 18
 Baldwin, J. A., Phillips, M. M., & Terlevich, R. 1981, *PASP*, **93**, 5
 Bannister, K. W., Deller, A. T., Phillips, C., et al. 2019, *Sci*, **365**, 565
 Bassa, C. G., Tendulkar, S. P., Adams, E. A. K., et al. 2017, *ApJL*, **843**, L8
 Becker, R. H., White, R. L., & Helfand, D. J. 1995, *ApJ*, **450**, 559
 Belczynski, K., Perna, R., Bulik, T., et al. 2006, *ApJ*, **648**, 1110
 Berger, E. 2009, *ApJ*, **690**, 231
 Bhandari, S., Bannister, K. W., Lenc, E., et al. 2020a, *ApJL*, **901**, L20
 Bhandari, S., Keane, E. F., Barr, E. D., et al. 2018, *MNRAS*, **475**, 1427
 Bhandari, S., Sadler, E. M., Prochaska, J. X., et al. 2020b, *ApJL*, **895**, L37
 Blanchard, P. K., Berger, E., & Fong, W.-f. 2016, *ApJ*, **817**, 144
 Bloom, J. S., Kulkarni, S. R., & Djorgovski, S. G. 2002, *AJ*, **123**, 1111
 Bloom, J. S., Sigurdsson, S., & Pols, O. R. 1999, *MNRAS*, **305**, 763
 Bochenek, C., Kulkarni, S., Ravi, V., et al. 2020a, *ATel*, **13684**, 1
 Bochenek, C. D., Ravi, V., Belov, K. V., et al. 2020b, *arXiv:2005.10828*
 Brinchmann, J., Pettini, M., & Charlot, S. 2008, *MNRAS*, **385**, 769
 Brown, W. R., Geller, M. J., Fabricant, D. G., & Kurtz, M. J. 2001, *AJ*, **122**, 714
 Bruzual, G., & Charlot, S. 2003, *MNRAS*, **344**, 1000
 Calzetti, D., Armus, L., Bohlin, R. C., et al. 2000, *ApJ*, **533**, 682
 Cappellari, M. 2017, *MNRAS*, **466**, 798
 Chabrier, G. 2003, *PASP*, **115**, 763
 Chambers, K. C., Magnier, E. A., Metcalfe, N., et al. 2016, *arXiv:1612.05560*
 Chatterjee, S., Law, C. J., Wharton, R. S., et al. 2017, *Natur*, **541**, 58
 Chen, G., Ravi, V., & Lu, W. 2020, *ApJ*, **897**, 146
 CHIME/FRB Collaboration, Amiri, M., Bandura, K., et al. 2018, *ApJ*, **863**, 48
 CHIME/FRB Collaboration, Andersen, B. C., Bandura, K., et al. 2019, *ApJL*, **885**, L24
 Chittidi, J. S., Simha, S., Mannings, A., et al. 2020, *arXiv:2005.13158*
 Cid Fernandes, R., Stasińska, G., Schlickmann, M. S., et al. 2010, *MNRAS*, **403**, 1036
 Cordes, J. M., & Chatterjee, S. 2019, *ARA&A*, **57**, 417
 Cross, N. J. G., Collins, R. S., Mann, R. G., et al. 2012, *A&A*, **548**, A119
 Dale, D. A., Helou, G., Magdis, G. E., et al. 2014, *ApJ*, **784**, 83
 Davidzon, I., Ilbert, O., Laigle, C., et al. 2017, *A&A*, **605**, A70
 Day, C. K., Deller, A. T., Shannon, R. M., et al. 2020, *MNRAS*, **497**, 3335
 Eftekhari, T., & Berger, E. 2017, *ApJ*, **849**, 162
 Finkelstein, S. L., Ryan, R. E. J., Papovitch, C., et al. 2015, *ApJ*, **810**, 71
 Fitzpatrick, E. L., & Massa, D. 2007, *ApJ*, **663**, 320
 Fong, W., & Berger, E. 2013, *ApJ*, **776**, 18
 Fong, W., Berger, E., & Fox, D. B. 2010, *ApJ*, **708**, 9
 Fonseca, E., Andersen, B. C., Bhardwaj, M., et al. 2020, *ApJL*, **891**, L6
 Fruchter, A. S., Levan, A. J., Strolger, L., et al. 2006, *Natur*, **441**, 463
 Fryer, C., & Kalogera, V. 1997, *ApJ*, **489**, 244
 Fynbo, J. P. U., Jakobsson, P., Prochaska, J. X., et al. 2009, *ApJS*, **185**, 526
 Hirschauer, A. S., Salzer, J. J., Janowiecki, S., & Wegner, G. A. 2018, *AJ*, **155**, 82
 Hogg, D. W., Pahre, M. A., McCarthy, J. K., et al. 1997, *MNRAS*, **288**, 404
 James, C. W., Osłowski, S., Flynn, C., et al. 2020, *MNRAS*, **495**, 2416
 Kashiyama, K., Ioka, K., & Mészáros, P. 2013, *ApJL*, **776**, L39
 Kauffmann, G., Heckman, T. M., Tremonti, C., et al. 2003, *MNRAS*, **346**, 1055
 Keating, L. C., & Pen, U.-L. 2020, *MNRAS*, **496**, L106
 Kelly, P. L., & Kirshner, R. P. 2012, *ApJ*, **759**, 107
 Kennicutt, R. C. J. 1998, *ARA&A*, **36**, 189
 Kewley, L. J., Nicholls, D. C., & Sutherland, R. S. 2019, *ARA&A*, **57**, 511
 Kothes, R., Sun, X., Gaensler, B., & Reich, W. 2018, *ApJ*, **852**, 54
 Kumar, P., Shannon, R. M., Flynn, C., et al. 2020, *MNRAS*, in press (doi:10.1093/mnras/staa3436)
 Lacy, M., Baum, S. A., Chandler, C. J., et al. 2020, *PASP*, **132**, 035001
 Law, C. J., Bower, G. C., Burke-Spolaor, S., et al. 2018, *ApJS*, **236**, 8
 Law, C. J., Butler, B. J., Prochaska, J. X., et al. 2020, *ApJ*, **899**, 161
 Li, Y., & Zhang, B. 2020, *ApJL*, **899**, L6
 Li, Y., Zhang, B., Nagamine, K., & Shi, J. 2019, *ApJL*, **884**, L26
 Licquia, T. C., & Newman, J. A. 2015, *ApJ*, **806**, 96
 Lo Faro, B., Buat, V., Roehly, Y., et al. 2017, *MNRAS*, **472**, 1372
 Lorimer, D. R., Bailes, M., McLaughlin, M. A., Narkevic, D. J., & Crawford, F. 2007, *Sci*, **318**, 777
 Lyman, J. D., Levan, A. J., Tanvir, N. R., et al. 2017, *MNRAS*, **467**, 1795
 Macquart, J.-P., Bailes, M., Bhat, N. D. R., et al. 2010, *PASA*, **27**, 272
 Macquart, J. P., Prochaska, J. X., McQuinn, M., et al. 2020, *Natur*, **581**, 391
 Maiolino, R., & Mannucci, F. 2019, *A&ARv*, **27**, 3
 Maiolino, R., Nagao, T., Grazian, A., et al. 2008, *A&A*, **488**, 463
 Marcote, B., Nimmo, K., Hessels, J. W. T., et al. 2020, *Natur*, **577**, 190
 Margalit, B., Berger, E., & Metzger, B. D. 2019, *ApJ*, **886**, 110
 Margalit, B., & Metzger, B. D. 2018, *ApJL*, **868**, L4
 Marnoch, L., Ryder, S. D., Bannister, K. W., et al. 2020, *A&A*, **639**, A119
 Martin, D. C., Wyder, T. K., Schiminovich, D., et al. 2007, *ApJS*, **173**, 342
 McQuinn, M. 2014, *ApJL*, **780**, L33
 Metzger, B. D., Berger, E., & Margalit, B. 2017, *ApJ*, **841**, 14
 Moriya, T. J. 2016, *ApJL*, **830**, L38
 Moustakas, J., Coil, A. L., Aird, J., et al. 2013, *ApJ*, **767**, 50
 Nicholl, M., Williams, P. K. G., Berger, E., et al. 2017, *ApJ*, **843**, 84
 Noll, S., Burgarella, D., Giovannoli, E., et al. 2009, *A&A*, **507**, 1793
 Nugent, A. E., Fong, W.-f., Dong, Y., et al. 2020, *arXiv:2007.10372*
 Oke, J. B., Cohen, J. G., Carr, M., et al. 1995, *PASP*, **107**, 375
 Palmerio, J. T., Vergani, S. D., Salvaterra, R., et al. 2019, *A&A*, **623**, A26
 Peng, C. Y., Ho, L. C., Impey, C. D., & Rix, H.-W. 2010, *AJ*, **139**, 2097
 Perley, D. A., Tanvir, N. R., Hjorth, J., et al. 2016, *ApJ*, **817**, 8
 Petroff, E., Burke-Spolaor, S., Keane, E. F., et al. 2017, *MNRAS*, **469**, 4465
 Petroff, E., Hessels, J. W. T., & Lorimer, D. R. 2019, *A&ARv*, **27**, 4
 Planck Collaboration, Ade, P. A. R., Aghanim, N., et al. 2016, *A&A*, **594**, A13
 Platts, E., Prochaska, J. X., & Law, C. J. 2020, *ApJL*, **895**, L49
 Platts, E., Weltman, A., Walters, A., et al. 2019, *PhR*, **821**, 1
 Prieto, J. L., Stanek, K. Z., & Beacom, J. F. 2008, *ApJ*, **673**, 999
 Prochaska, J. X., Hennawi, J. F., Westfall, K. B., et al. 2020, *pypet/Pypelt: Release 1.0.0*, Zenodo, doi:10.5281/zenodo.3743493
 Prochaska, J. X., Macquart, J.-P., McQuinn, M., et al. 2019a, *Sci*, **366**, 231
 Prochaska, J. X., Simha, S., & Tejos, N. 2019b, *ATel*, **13144**, 1
 Prochaska, J. X., & Zheng, Y. 2019, *MNRAS*, **485**, 648
 Ravi, V., Catha, M., D'Addario, L., et al. 2019, *Natur*, **572**, 352
 Reddy, N. A., & Steidel, C. C. 2009, *ApJ*, **692**, 778
 Savaglio, S., Glazebrook, K., & Le Borgne, D. 2009, *ApJ*, **691**, 182
 Schlafly, E. F., & Finkbeiner, D. P. 2011, *ApJ*, **737**, 103
 Schlegel, D. J., Finkbeiner, D. P., & Davis, M. 1998, *ApJ*, **500**, 525
 Scholz, P., & Chime/Frb Collaboration 2020, *ATel*, **13681**, 1
 Schulze, S., Chapman, R., Hjorth, J., et al. 2015, *ApJ*, **808**, 73
 Schulze, S., Yaron, O., Sollerman, J., et al. 2020, *arXiv:2008.05988*
 Simha, S., Burchett, J. N., Prochaska, J. X., et al. 2020, *ApJ*, **901**, 134
 Singh, R., van de Ven, G., Jahnke, K., et al. 2013, *A&A*, **558**, A43
 Spitler, L. G., Scholz, P., Hessels, J. W. T., et al. 2016, *Natur*, **531**, 202
 Steidel, C. C., Rudie, G. C., Strom, A. L., et al. 2014, *ApJ*, **795**, 165
 Stern, J., & Laor, A. 2012, *MNRAS*, **423**, 600
 Strateva, I., Ivezić, Ž., Knapp, G. R., et al. 2001, *AJ*, **122**, 1861
 Taggart, K., & Perley, D. 2019, *arXiv:1911.09112*
 Tendulkar, S. P., Bassa, C. G., Cordes, J. M., et al. 2017, *ApJL*, **834**, L7
 The CHIME/FRB Collaboration, Andersen, B. C., Bandura, K. M., et al. 2020, *arXiv:2005.10324*
 Thomas, A. D., Kewley, L. J., Dopita, M. A., et al. 2018, *ApJL*, **861**, L2
 Thornton, D., Stappers, B., Bailes, M., et al. 2013, *Sci*, **341**, 53
 Tunnicliffe, R. L., Levan, A. J., Tanvir, N. R., et al. 2014, *MNRAS*, **437**, 1495
 Vergani, S. D., Salvaterra, R., Japelj, J., et al. 2015, *A&A*, **581**, A102
 Willmer, C. N. A., Faber, S. M., Koo, D. C., et al. 2006, *ApJ*, **647**, 853
 Wolf, C., Meisenheimer, K., Rix, H. W., et al. 2003, *A&A*, **401**, 73
 Wolfe, A. M., Gawiser, E., & Prochaska, J. X. 2005, *ARA&A*, **43**, 861
 Woosley, S. E., & Heger, A. 2006, *ApJ*, **637**, 914
 Yan, R., & Blanton, M. R. 2012, *ApJ*, **747**, 61
 Yoon, S. C., Langer, N., & Norman, C. 2006, *A&A*, **460**, 199